

Prediction of Explosive Cylinder Tests Using Equations of State from the PANDA Code

Gerald I. Kerley
Computational Physics and Mechanics Department
Sandia National Laboratories
Albuquerque, NM 87185

Tracy L. Christian-Frear RE/SPEC Inc. 4775 Indian School Rd., NE, Suite 300 Albuquerque, NM 87110

Abstract

The PANDA code is used to construct tabular equations of state (EOS) for the detonation products of 24 explosives having CHNO compositions. These EOS, together with a reactive burn model, are used in numerical hydrocode calculations of cylinder tests. The predicted detonation properties and cylinder wall velocities are found to give very good agreement with experimental data. Calculations of flat plate acceleration tests for the HMX-based explosive LX14 are also made and shown to agree well with the measurements. The effects of the reaction zone on both the cylinder and flat plate tests are discussed. For TATB-based explosives, the differences between experiment and theory are consistently larger than for other compositions and may be due to nonideal (finite diameter) behavior.

MASTER

zþ

Contents

Co	ntents		4		
Lis	t of F	igures	5		
		ables			
1.	Introduction				
	1.1	Background	6		
	1.2	The Cylinder Test - a Review	6		
	1.3	Theoretical EOS Model	7		
	1.4	Scope of Report	8		
2.	Calci	ılational Model	9		
	2.1	EOS Tables for Detonation Products	9		
	2.2	CTH Calculations	10		
	2.3	Burn Model	11		
3.	Results				
	3.1	Detonation Properties			
	3.2	Cylinder Tests	15		
	3.3	Plate Acceleration Tests	21		
4.	Sumr	nary and Conclusions	27		
Re	ferenc	es	28		
Аp	pendi	x A: PANDA Input File for PBX9404	.32		
Ap	pendi	x B: CTH Input File for PBX9404 Cylinder Test	34		
Ap	pendi	C: CTH Input File for LX14 Plate Acceleration Test	38		
Dis	stribut	ion	41		

List of Figures

Fig. 1.	Results for a 1-in cylinder test of PBX9404	12
Fig. 2.	Detonation velocity of TATB-based explosives as a function of reciprocal charadius	
Fig. 3.	Velocity vs. radius for PBX9404 cylinder test	16
Fig. 4.	Velocity and radius vs. time for PBX9404 cylinder test	16
Fig. 5.	Results for 1-in and 2-in cylinder tests of LX-14	17
Fig. 6.	Cylinder test data for three HMX-based explosives	18
Fig. 7.	Cylinder test results for RDX-TNT mixtures	18
Fig. 8.	Cylinder test results for HNS at various loading densities	19
Fig. 9.	Cylinder test results for PETN and NM	19
Fig. 10.	Results for 1-in and 2-in cylinder tests of PBX9502	20
Fig. 11.	LX14 flat plate tests #9633 and 9634 of Ref. [21]	23
Fig. 12.	. Initial acceleration of copper plate for experiments reported in Ref. [21]	24
Fig. 13.	. Impedance matching diagram for interaction of copper plate with LX14 explosive	
Fig. 14.	. LX14 flat plate test #9643 of Ref. [21]	26
	. LX14 flat plate test #9526 of Ref. [21]	
	List of Tables	
Table 1	Compositions and heats of formation of explosives	9
Table 2	Experimental and calculated detonation properties	14
Table 3	Summary of copper cylinder wall velocity calculations	22

1. Introduction

1.1 Background

The accurate *a priori* prediction of equations of state (EOS) for the detonation products of high explosives (HE) has been one of the principal aims of explosives research for many years. The empirical JWL (Jones-Wilkins-Lee) EOS formula [1], although very popular and useful, does not provide this predictive capability because it must be fit to experimental data for each new explosive composition. Theoretical "chemical" EOS models, on the other hand, have been shown to give reasonable predictions of explosive detonation properties [2]-[9]. Until recently, however, the chemical models did not offer enough accuracy to be satisfactory alternatives to JWL, even after the model parameters had been adjusted to fit experimental data [10].

To be truly viable as a predictive tool, a theoretical model should give accurate results for the following properties:

- 1. The steady-state detonation velocity, including its dependence upon loading density and systematic variations in chemical composition of the explosive.
- 2. The pressure and temperature at the Chapman-Jouguet (CJ) state, i.e. the point of complete decomposition at the end of the reaction zone. (These quantities usually cannot be determined as accurately as the detonation velocity [10].)
- 3. The expansion behavior of the detonation products behind the detonation front, normally studied using cylinder tests and other hydrodynamic experiments [1].
- 4. The overdriven Hugoniot, i.e. the shock properties of the detonation products compressed above the CJ point [11].

In this report we will consider a chemical model for calculating the EOS of explosive detonation products that was first presented at the Eighth Detonation Symposium [7]. This model is available in the PANDA code [12] and will be referred to here as "the PANDA model." References [7] and [8] showed that the PANDA model gives very good predictions of the detonation properties and the overdriven Hugoniots for explosives having CHNO compositions. We will show that it also gives good predictions for the expansion behavior by comparing it with cylinder test data for 24 explosives.

1.2 The Cylinder Test - a Review

A cylinder test measures the radial expansion of a stick of explosive that is enclosed in a metal tube and detonated at one end. The most common configuration used at Lawrence Livermore National Laboratory [1][10] employs a 30 cm length of explosive with a 1-in diameter, enclosed in a copper tube of thickness 0.26 cm. The radius of the tube as a function of time is recorded at a distance 21 cm from the point of detonation, using a streak camera. The velocity history of the expanding tube is especially important, because the

velocity is closely related to the energy of the expanding gases. Until recently, the velocity history was determined by differentiation of the radius vs. time curve. The velocity can now be determined more precisely using Fabry-Perot interferometers [10].

Experiments on larger diameter sticks have also been carried out to investigate time-dependent effects [1]. The results for most explosives satisfy hydrodynamic scaling, at least to within experimental error, showing that the 1-in test approximates infinite diameter behavior. In such cases, it is reasonable to conclude that the cylinder test results depend only on the detonation product EOS, i.e., that they are insensitive to reaction rate effects. However, some explosives with long reaction zones do exhibit diameter effects that are indicative of time-dependent behavior.

JWL EOS fits for explosive detonation products are usually determined by making hydrocode calculations of the cylinder test and adjusting the parameters until satisfactory agreement with measured velocity vs. radius curve is obtained [1][10]. The fit parameters are usually also constrained to match the experimental detonation velocity and pressure. The test data are normally obtained to 2.5-fold expansion of the cylinder, thereby defining the EOS to about 7-fold volume expansion. Since the products expand adiabatically, a single cylinder test only measures the adiabat through the CJ point for a single initial density. In principle, the detonation product EOS should be be capable of predicting the cylinder test results for any initial density. In practice, however, separate JWL fits have to be made for each case. This fact shows that the JWL formula, which assumes a constant specific heat and Grüneisen parameter, gives only an approximate representation of states off the CJ adiabat.

The importance of the cylinder test as a diagnostic tool is illustrated by the fact that theoretical EOS models frequently fail to give satisfactory predictions of the results. Souers and Kury [10] recently compared finite element calculations made using different EOS models with cylinder test data for 19 homogeneous explosives. All three theoretical models considered exhibited significant discrepancies (as high as 20-30% in some cases) with the cylinder test data. The predicted detonation velocities were much better. Hence the ability of a model to predict the CJ detonation properties does not guarantee its ability to predict the detonation product expansion.

1.3 Theoretical EOS Model

In the PANDA model, separate EOS tables are first constructed for each of the chemical species that are to be allowed in the detonation products. For CHNO compositions, the principal species are: CO_2 , N_2 , H_2O , CO, NO, NH_3 , CH_4 , H_2 , O_2 , HCOOH (formic acid), atomic N, O, and H, and three forms of condensed carbon - graphite, diamond, and liquid carbon. Fluid perturbation theory [13] is used for all species except for solid carbon. Next, the ideal mixing model is used to compute the thermodynamic functions for a mixture of these species, and the composition of the system is determined from assumption of chemical equilibrium. The same library of EOS tables for the chemical species is used for all explosive compositions. Hence the only input parameters required by PANDA are the chemical formula $C_wH_xN_yO_z$ and the heat of formation for the unreacted explosive. (The model has not yet been extended to allow elements other than C, H, N, and O.)

The principal conclusions of previous work are as follows.

- The ideal mixing approximation gives surprisingly accurate results, not only for detonation products, but also when compared with Monte Carlo simulations of mixtures [8][14]. As a result, more realistic EOS can be used for complicated chemical species than would be possible with mixture theories based upon simple intermolecular pair potentials.
- Formic acid is a very important reaction product for explosives having a negative oxygen balance, especially for HMX and RDX. The atomic forms of nitrogen and oxygen are are also important in some cases.
- A three-phase model of condensed carbon (graphite, diamond, and liquid) is necessary for explaining variations in detonation properties with changes in composition and loading density. In particular, the transition from graphite to diamond in TNT at high densities was first predicted in Ref. [7].
- In addition to giving good *a priori* predictions of detonation velocities, pressures, and temperatures, the model gives very good agreement with Hugoniots for explosives in the overdriven shock region and Hugoniots of non-explosive CHNO compounds at pressures high enough to create dissociation.

1.4 Scope of Report

Hydrocode calculations of cylinder tests were made for 24 explosives for which experimental data were available. Calculations were also made for plate impact tests of LX14.

Various features of the computational model are discussed in Sec. 2 - the EOS tables for the detonation products (Sec. 2.1), the hydrocode input (Sec. 2.2), and the burn model used to propagate the detonation wave along the cylinder (Sec. 2.3).

The results are discussed in Sec. 3. The calculated detonation properties, presented in Sec. 3.1, are shown to agree very well with experimental data for all of the explosives considered. For the detonation velocities, which are the most accurately known detonation properties, the predictions are within ~1.5% of the measurements, on the average. The cylinder test results are presented in Sec 3.2. The calculated cylinder wall velocities are shown to agree with the experimental data to within ~2.6%, on the average. In Sec. 3.3, it is shown that the model also gives good predictions of the flat plate impact tests for LX14.

2. Calculational Model

2.1 EOS Tables for Detonation Products

EOS tables for the detonation products of the 24 explosives studied were made using the mixture/chemical equilibrium model in the PANDA code (version 2.06) [12]. The explosive compositions and heats of formation, obtained from Refs. [10], [15], and [16], are listed in Table 1. For composites and mixtures, the chemical formula was defined in terms of an arbitrary mass of explosive [15], since only the relative CHNO ratios affect the EOS. Three of the explosives considered (LX-09, PBX9404, and PBX9502) contain small amounts of elements other than C, H, N, and O These additional elements were ignored in the present work.

TABLE 1: Compositions and heats of formation of explosives.

Explosive ^a	Formula ^b	ΔH _f °(298K) (MJ/kg)
BTF	C[6]N[6]O[6]	+2.387
Comp B, Grade A (63% RDX/36% TNT)	C[2.03]H[2.64]N[2.18]O[2.67]	+0.0538
Cyclotol, 77/23 (77% RDX/23% TNT)	C[1.75]H[2.59]N[2.38]O[2.69]	+0.145
HMX	C[4]H[8]N[8]O[8]	+0.2531
HNB	C[6]N[6]O[12]	+0.1887
HNO ₃ #1 (60% HNO ₃ /40% DNB)	C[1.2]H[1.6]N[1.2]O[3.2]	-1.711
HNO ₃ #2 (60% HNO ₃ /30% DNB/10% RDX)	C[1.0]H[1.6]N[1.3]O[3.3]	-1.676
HNS	C[14]H[6]N[6]O[12]	+0.174
LX09 (93% HMX/4.6% pDNPA/2.4% FEFO)	C[1.43]H[2.74]N[2.59]O[2.72]F[.02]	+0.0838
LX14 (95.5%HMX/4.5% Es)	C[1.52]H[2.92]N[2.59]O[2.66]	+0.0628
NM	C[1]H[3]N[1]O[2]	-1.849
NNE (39% NM/56% NP/5% ED)	C[2.0]H[5.2]N[1.1]O[1.9]	-1.908
PBX9011 (90% HMX/10% Es)	C[1.73]H[3.18]N[2.45]O[2.61]	-0.170
PBX9404 (94% HMX/3% NC/3% CEF)	C[1.40]H[2.75]N[2.57]O[2.69]Cl[.03]P[.01]	+0.00331
PBX9501 (95% HMX/2.5% Es/2.5% BDNP)	C[1.47]H[2.86]N[2.60]O[2.69]	+0.0954
PBX9502 (95% TATB/5% Kel-F)	C[2.30]H[2.23]N[2.21]O[2.21]CI[.038]F[.13	-0.8715
PETN	C[5]H[8]N[4]O[12]	-1.7031
RX-23-AA (79% HyN/21% Hy)	H[4.6]N[2.6]O[1.7]	-1.824
RX-23-AB (69% HyN/5% Hy/26% H ₂ O)	H[3.2]N[1.2]O[1.6]	-5.415
RX-23-AC (32% HyN/68% Hy)	H[4.1]N[2.1]O[0.4]	+0.1635
TATB	C[6]H[6]N[6]O[6]	-0.5971
TNGU	C[4]H[2]N[8]O[10]	+0.1559
TNM	C[1]N[4]O[8]	+0.276
TNT	C[7]H[5]N[3]O[6]	-0.295

^a The following abbreviations were used in specifying the compositions for the mixtures: Es=Estane; Hy=hydrazine; HyN = hydrazine nitrate.

^b Elements other than C, H, N, and O were not included in making the EOS tables.

The PANDA input file for PBX9404, which is typical of that used in all cases, is shown in Appendix A. The detonation products were treated as a mixture of 16 chemical species as described in Sec 1.3. EOS tables for these species had previously been constructed and saved on a data file, as described in Ref. [8]. This same file was used for all explosives, so that only the chemical formula $C_wH_xN_yO_z$ and the heat of formation of the unreacted explosive differed from case to case.

The detonation product EOS were tabulated on a rectangular density-temperature grid covering the range from $0.01 \le \rho \le 5.0$ g/cm³ and from $10^3 \le T \le 10^4$ K, equally spaced in $\log(\rho)$ and $\log(T)$, along with points at $\rho=0$ and T=298K. For some explosives, extra densities and temperatures were added in the vicinity of the CJ point to improve resolution and give better results for the detonation properties.

2.2 CTH Calculations

Numerical calculations of the cylinder tests were made using the Eulerian code CTH [17]-[20]. The CTH input file for PBX9404, listed in Appendix B, is typical of those used for tests with a 1-in (2.54 cm) diameter and 0.26 cm wall thickness. A 15-cm length of explosive was used in calculations of the 1-in diameter tests. The radial velocity of the cylinder wall was recorded using tracer particles located near the outside of the copper tube at 7.0, 8.0, and 9.0 cm along the axis from the initiation surface. In order to simulate the experimental conditions, the tracers were only allowed to move in the radial direction; their axial positions were held constant using the "FIXED=Y" option. The fact that the tracers gave nearly identical results for the cylinder wall velocity history showed that steady state conditions had been reached at these positions. For calculations of 2-in cylinder tests, an additional length of 2-5 cm was needed to obtain steady state conditions.

Good resolution of the copper cylinder wall motion was obtained using 0.02-cm zones in the radial direction (13 zones across the tube wall). To minimize computing time, 0.05-cm thick zones were used in the axial direction from 5.0 to 10.0 cm (the region encompassing the tracers), with graded zones at the beginning and end of the stick. Note that this zoning scheme leads to cells with a 2.5:1 aspect ratio in the central part of the problem, a condition which can give poor results in Eulerian calculations and is *not* recommended for general use. Nevertheless, the results were found to be satisfactory in this work because of the fact that the axial and radial flows are nearly independent in cylinder tests. To test the zoning approximations, calculations also were made using 1:1 aspect ratios, using both 0.02-cm and 0.05-cm zone sizes. These tests showed that the use of non-square zoning did not cause any appreciable error. The zone size studies show that the zoning used here is more than adequate to match the precision of most of the experimental measurents. However, much finer zoning would be needed to resolve the ringing behavior in the early time motion with the precision that can be obtained using Fabry-Perot interferometry [21].

The CTH calculations of the flat plate experiments [21], which are discussed in Sec. 3.3, required much finer zoning than did the cylinder tests because the copper thicknesses were much smaller. A sample CTH input file for one of the plate tests is listed in Appendix C, and further details are given in Sec. 3.3.

The copper, in both the cylinder and flat plate tests, was treated using the Mie-Grüneisen EOS and the elastic-perfectly plastic model with a yield strength of 0.35 GPa and Poisson's ratio of 0.35. To test this approximation, a few calculations were also made with more sophisticated constitutive models [43][44]; the results did not differ appreciably from those obtained with the simpler model.

2.3 Burn Model

Although the cylinder expansion behavior is determined primarily by the detonation product EOS, reaction rate properties, such as the structure of the reaction zone and curvature of the wave front, can also influence the results. In this work, the explosives were initiated by a 1.3-cm long "booster" and burned using the history variable reactive burn model (HVRB) [20]. The detonation of the booster was modeled using the JWL EOS and the CTH programmed burn option [19].

In the HVRB model, the EOS for the partially reacted explosive is given by the expressions [20]

$$P(\rho, T, \lambda) = (1 - \lambda) P_i(\rho, T) + \lambda P_f(\rho, T)$$
(1)

and

$$E(\rho, T, \lambda) = (1 - \lambda) E_i(\rho, T) + \lambda E_f(\rho, T).$$
 (2)

Here P_f and E_f describe the detonation products and are calculated from the tabular EOS discussed in Sec. 2.1. P_i and E_i describe the unreacted explosive and are calculated from the Mie-Grüneisen formula. The extent of reaction λ is given as a function of time t by

$$\lambda(t) = \min(1, \phi^M), \tag{3}$$

and

$$\phi(t) = \frac{1}{\tau_0} \int_0^t \left(\frac{P - P_i}{P_r}\right)^z d\tau, \tag{4}$$

where the integrand in Eq. (4) is set to zero for $P < P_i$. The constants P_p , z, M, and P_i for each explosive are calibrated from experimental data, and $\tau_0=1.0$ µsec. Where possible, the HVRB parameters used in the cylinder tests calculations were determined by calibrating the model to wedge test data [15][16], as described in Ref. [20]. For explosives where no wedge tests were available, the parameters were estimated from other initiation data. These calibrations will be discussed in separate reports.

In order to evaluate the importance of reaction rate effects on the numerical results, calculations of a 1-in cylinder test of PBX9404 were made using the JWL EOS with three different burn models. The results are compared with one another and with experimental data [16] [22] in Fig. 1. During the early part of the expansion, the calculation using the HVRB

model (solid line) gives higher expansion velocities than the one using programmed burn (dotted line). The difference between the two models decreases at later times, although the HVRB velocity continues to be about 1% higher out to an expansion of 2.0 cm.

The differences are due, at least in part, to reaction zone effects. The von Neumann spike, which appears only in the HVRB calculation, gives a somewhat higher initial push to the copper tube. A calculation using the CJ volume burn (CJVB) model [20] is also shown in Fig. 1 (dashed line). The CJVB parameters used here were selected so that the detonation wave had no reaction zone; consequently, the results are close to those for programmed burn.

The above results tend to support the usual assumption that the principal features of the cylinder wall motion are determined by the detonation product EOS. However, they show that reaction rate effects do influence the early time behavior and can increase the overall velocity by as much as 1%, even at later times. The reactive burn model was much more important in calculations of the flat plate experiments than in the cylinder tests, because the copper thicknesses were so much smaller. This problem is discussed in Sec. 3.3.

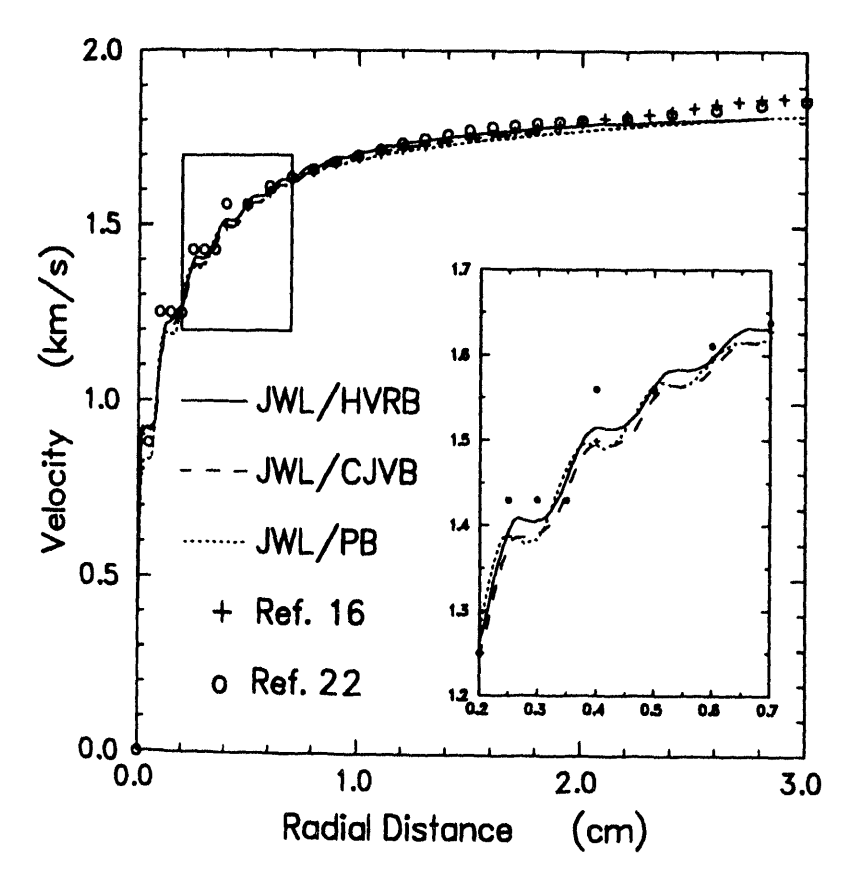


Fig. 1. Results for a 1-in cylinder test of PBX9404. The JWL EOS was used for the detonation products, and the detonation wave was propagated using programmed burn (PB), CJ volume burn (CJVB), and history variable reactive burn (HVRB). The inset figure gives an enlarged view of the region marked by the square. The discrete points are experimental data, as marked.

3. Results

3.1 Detonation Properties

Table 2 gives the experimental and calculated detonation velocities, pressures, and temperatures for the 24 explosives considered in this work. The model gives especially good agreement with the experimental detonation velocities, the most accurately measured quantities. When the results for TATB and PBX9502 are excluded, the average difference between the calculated and experimental values is only -0.1%, with a standard deviation of 1.4%, which is comparable to the scatter observed in the experimental measurements.

As previously noted in Ref. [7], the calculated detonation velocities for TATB-based explosives are higher than the experimental values by about 5%. In Sec. 3.2 it is shown that a comparable discrepancy is also obtained for the cylinder wall expansion velocities. These differences are well outside those obtained for the other explosives and are not yet fully understood. However, some of the discrepancy is undoubtedly due to nonideal behavior. The measured detonation velocity for 95% TATB/5% Kel-F [23][24] is shown as a function of the reciprocal charge radius in Fig. 2. The curve is concave upward at large radii, and the ideal (infinite diameter) value has not been attained even for charge diameters as large as 13 cm. This behavior is different from that seen in other explosives [23], and the infinite diameter value cannot be obtained accurately by the usual extrapolation methods. Therefore, the ideal detonation velocities of TATB and for PBX9502 must be higher than the values given in Table 2, i.e. closer to the model predictions.

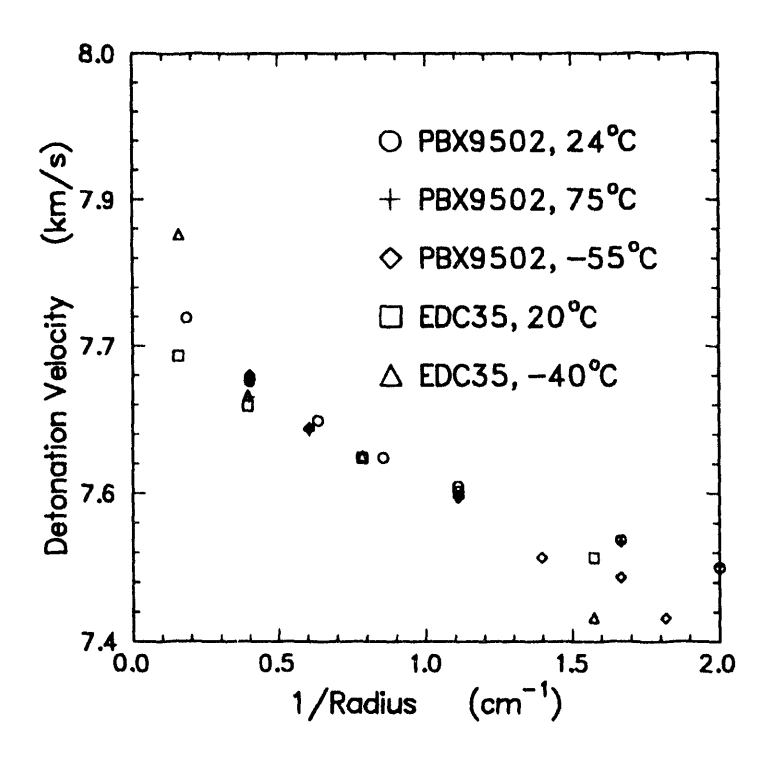


Fig. 2. Detonation velocity of TATB-based explosives as a function of reciprocal charge radius; PBX9502 - [23], EDC35 - [24].

TABLE 2: Experimental and calculated detonation properties.

	Initial		Detonation Properties						
Explosive	Density	D _{CJ} (km/s)		P _{CJ} (GPa)		$T_{CJ}(K)$		Refs.	
	(g/cm^3)	expt.	calc.	expt.	calc.	expt.	calc.		
BTF	1.860	8.49	8.54	36.0	31.4	-	4480.	[15]	
Comp B (Gr. A)	1.720	7.99	7.85	29.5	27.4	-	3620.	[15]	
Cyclotol (77/23)	1.743	8.25	8.18	31.3	29.0	-	3740.	[16]	
HMX	1.891	9.11	9.10	39.0	38.6	-	3660.	[16][26]	
HMX	1.630	8.08	8.06	27.5	27.7	4300.	3950.	[16][26][35	
HMX	1.200	6.59	6.73	15.0	15.3	-	4330.	[16][26]	
HNB	1.965	9.34	9.26	42.5	38.5	-	5080.	[10]	
HNO ₃ #1	1.542	7.23	7.44	21.0	20.4	-	4620.	[10]	
HNO ₃ #2	1.560	7.26	7.37	20.5	19.5	-	4160.	[10]	
HNS	1.681	7.08	7.00	23.0	23.5	-	3700.	[10][27]	
HNS	1.402	6.34	6.23	16.0	16.2	-	3960.	[10][27]	
HNS	1.001	5.10	5.18	7.2	7.18	-	3830.	[10][27]	
LX09	1.840	8.81	8.81	37.7	35.0	-	3680.	[15]	
LX14	1.835	8.83	8.75	37.0	33.8	-	3580.	[15]	
NM	1.130	6.21	6.22	13.4	11.8	3470.	3570.	[28][29][35	
NNE	1.034	5.31	5.38	9.0	7.57	-	2720.	[10]	
PBX9011	1.770	8.50	8.33	29.8	29.4	-	3420.	[16]	
PBX9404	1.846	8.78	8.84	35.6	35.2	-	3630.	[28][29]	
PBX9501	1.832	8.80	8.77	-	34.0	-	3640.	[28]	
PBX9502	1.890	>7.73 ^a	8.10	28.9	26.4	-	2730.	[23][29]	
PETN	1.763	8.27	8.29	31.5	30.1	42 00.	4200.	[30][33]	
PETN	1.620	7.85	7.78	26.0	25.4	4400.	4380.	[30][35]	
PETN	1.510	7.47	7.40	21.9	21.5	-	4480.	[30]	
PETN	1.230	6.46	6.37	13.8	12.8	-	4670.	[30]	
RX-23-AA	1.424	8.64	8.55	21.0	23.0	2900.	2800.	[10][34]	
RX-23-AB	1.356	7.48	7.39	17.0	15.8	4000.	2360.	[10][34]	
RX-23-AC	1.136	7.88	7.80	18.1	15.1	2180.	2230.	[10][34]	
TATB	1.860	>7.75 ^a	8.07	25.9	26.9	-	2940.	[16]	
TNGU	1.885	-	9.09	37.0	35.7	-	4250.	[10]	
TNM	1.650	6.45	6.67	15.5	15.6	2840.	2450.	[10][34]	
TNT	1.632	6.94	6.94	21.6	26.1	-	3660.	[10][31]	
TNT	1.400	6.33	6.28	16.0	13.8	3520.	3690.	[31][32][37	
average difference	-0.1% ^b		-3.9%		-6.3%				
standard, deviation			1.4% ^b		8.1%		15.8%		

^a See discussion in the text and Refs. [23] and [24]
^b Values computed excluding detonation velocities of PBX9502 and TATB

The average difference between the calculated and experimental detonation pressures is -3.9%, with a standard deviation of 8.1%, all within typical experimental uncertainties. It has been shown that measurements of the detonation pressure are less accurate than those of the detonation velocity and that there are significant variations in the results obtained by different methods [10][25]. The difficulties are due in part to the fact that the CJ state, which is preceded by the von Neumann spike and immediately followed by the Taylor (release) wave, is not easy to pinpoint, even in numerical simulations. In fact, many of the "experimental" values given in Table 2 are only estimates based upon cylinder tests [10], which are not particularly sensitive to the detonation pressure [21]. These matters are discussed further in Sec. 3.3, where it is shown that the detonation pressure for LX14 is probably lower than the value given in Table 2.

Measurements of the detonation temperature are fewer and much less accurate than those of either the velocity or the pressure. The data for transparent liquids, especially ones having a small reaction zone, are the most reliable; measurements for solid explosives have additional complications due to being opaque and having hot spots [10]. For liquid NM, Refs. [35] and [36] report 13 experiments giving an average of 3470K, with a standard deviation of 190K and a total spread of 780K. Temperature measurements have also been reported for the liquids TNM, RX-23-AA, RX-23-AB, and RX-23-AC [34]. The reported measurements for solid PETN [33][35][36][38] show a spread of about 600K and appear to be reasonable and consistent for initial densities in the range 1.6<po<1.77. However, there is a larger spread in the reported data for the solids TNT and HMX [35][36][37][38]. Moreover, the measurements of Huisheng, et al. [38], for TNT and HMX at high initial densities, are inconsistent with the data for lower densities and need to be checked. The calculated detonation temperatures are well within the experimental uncertainties for all but one of the explosives shown in Table 2 - the experimental value for RX-23-AB, which is inconsistent with those for RX-23-AA and RX-23-AC, is likely to be erroneous [3].

3.2 Cylinder Tests

The calculated results for a 1-in cylinder test on PBX9404 [16][22] are shown in Figs. 3 and 4. Figure 3 compares the velocity vs. radius curves obtained using both the PANDA EOS and the JWL EOS with the experimental data. The two calculations are almost indistinguishable from one another and in excellent agreement with the measurements at early times. For radial expansions greater than 1.8 cm, the PANDA EOS predicts slightly higher velocities and gives better agreement with the data than JWL. For completeness, the velocity vs. time and radius vs. time curves for the PANDA calculation are shown in Figs. 4a and 4b, respectively. As expected, the agreement here is also excellent.

Calculations for LX14, another HMX-based explosive having a composition and properties similar to those of PBX9404, are shown in Fig. 5. Velocity vs. radius curves for both a 1-in test [16][21]and also a 2-in test [22] are shown in Fig. 5a. (The wall thickness was 0.26 cm in both cases.) Once again, the calculated results are in excellent agreement with the experimental data. Figure 5b compares the calculated velocity vs. time for the 2-in test with high precision measurements obtained using a Fabry-Perot interferometer [21]. Results obtained with both standard zoning (Δx =0.02 cm, Δy =0.05 cm) and finer zoning (Δx =0.01 cm, Δy =0.02 cm) are shown. The agreement with experiment is good, although

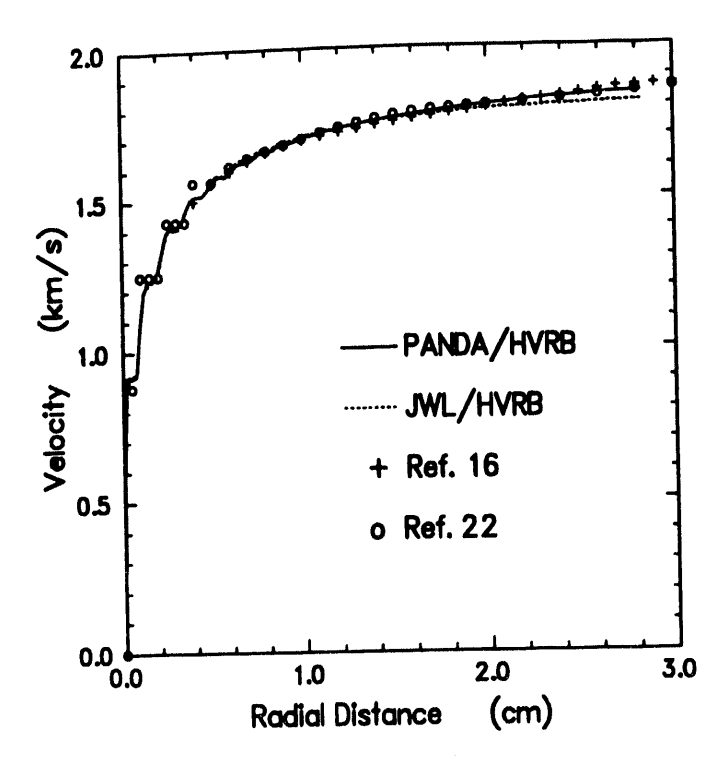


Fig. 3. Velocity vs. radius for PBX9404 cylinder test [16][22]. Calculations using both PANDA and JWL EOS are shown.

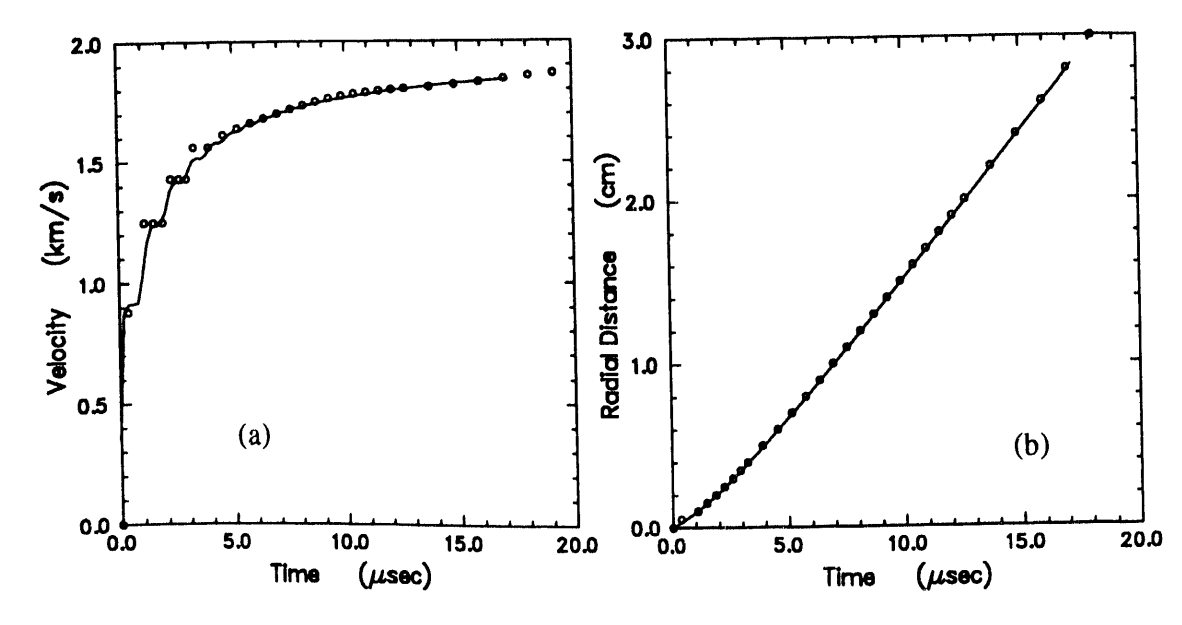


Fig. 4. Velocity vs time (a) and radius vs. time (b) for PBX9404 cylinder test [22]. (PANDA results only)

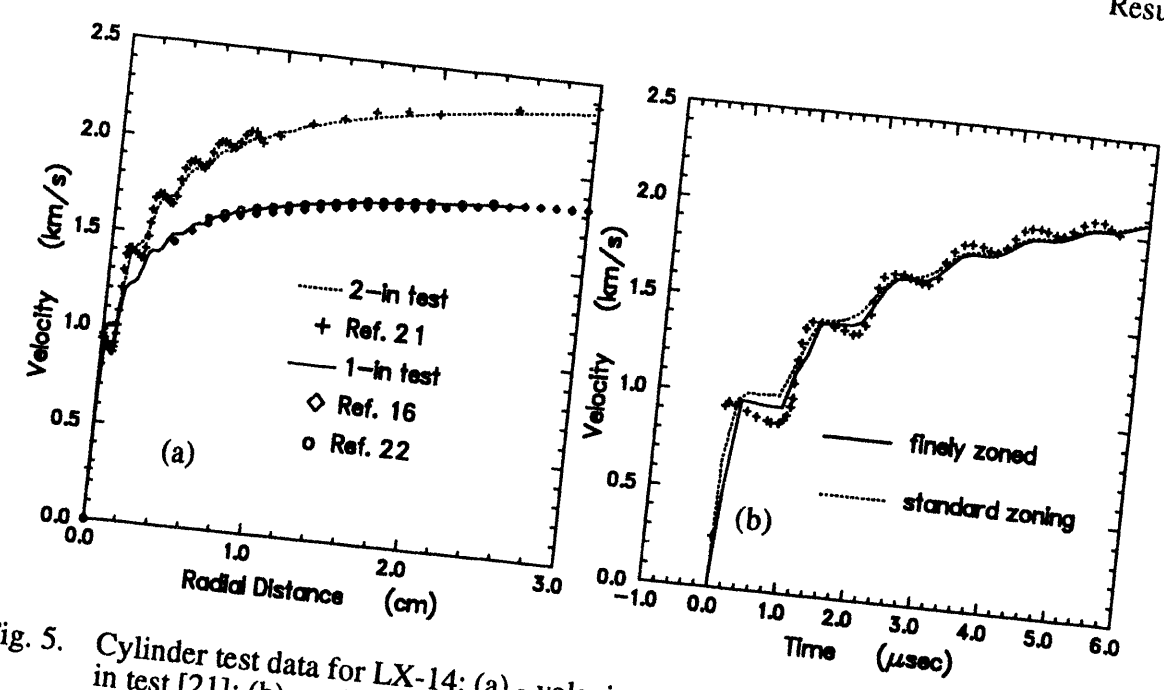


Fig. 5. Cylinder test data for LX-14: (a) - velocity vs. radius for 1-in test [16][22] and 2-in test [21].

even the more finely-zoned calculation does not resolve the velocity oscillations with as much precision as the measurements.

Figure 6 shows the effect of additive content on the cylinder test results for three HMX-based explosives - 100% HMX, PBX-9501 (95% HMX), and PBX9011 (90% HMX). The additives reduce the cylinder wall velocity of HMX by ~6% and ~10% for PBX9501 and PBX9011, respectively. The calculations agree quite well with the experimental data changes in chemical composition.

Figure 7 shows the cylinder test results for three RDX-TNT mixtures - pure TNT, Comp B, Grade A (64% RDX, 36% TNT), and Cyclotol (77% RDX, 23% TNT). Since no cylinder test data are available for RDX, the data for HMX are also shown. (The cylinder test results for RDX and HMX should be identical except for a small effect due to different loading densities.) Adding RDX to TNT increases the wall velocity by ~15% and ~20% ment with the experimental data [1] for all four cases, showing that the model accurately predicts the effects of variations in explosive composition.

Figure 8 shows cylinder test results for HNS at loading densities ranging from 1.0 to 1.68 g/cm³. (Note that all of the curves were computed using the same EOS table, instead of using a separate EOS fit for each density, as is usually done with the JWL formula.) The calculated wall velocities are slightly higher than the experimental ones [27] (by ~2% at the highest density and by ~4% at the lowest density). However, the model accurately predicts the drop in cylinder wall velocity with increasing porosity.

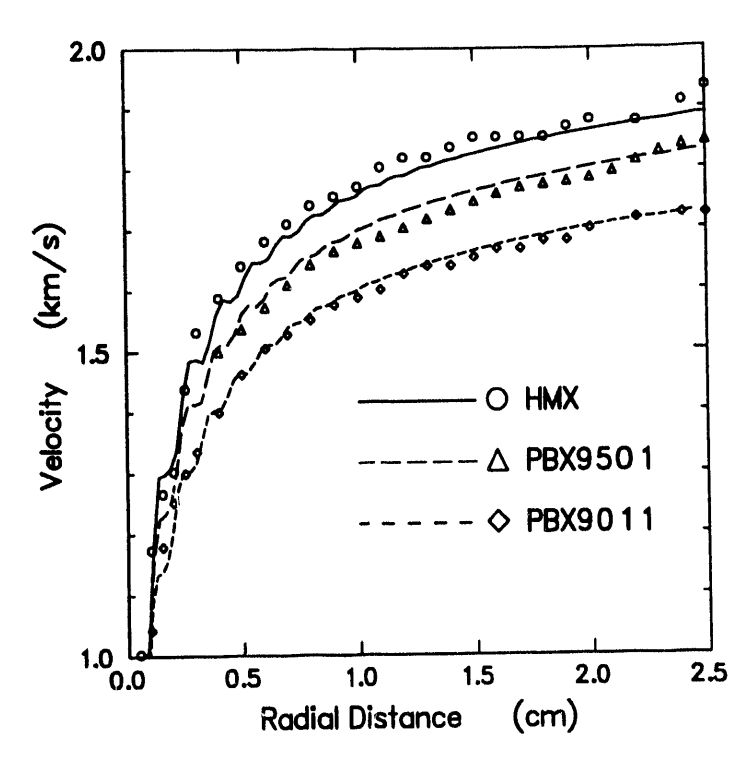


Fig. 6. Cylinder test data for three HMX-based explosives. Experimental data are from Refs. [1] and [16].

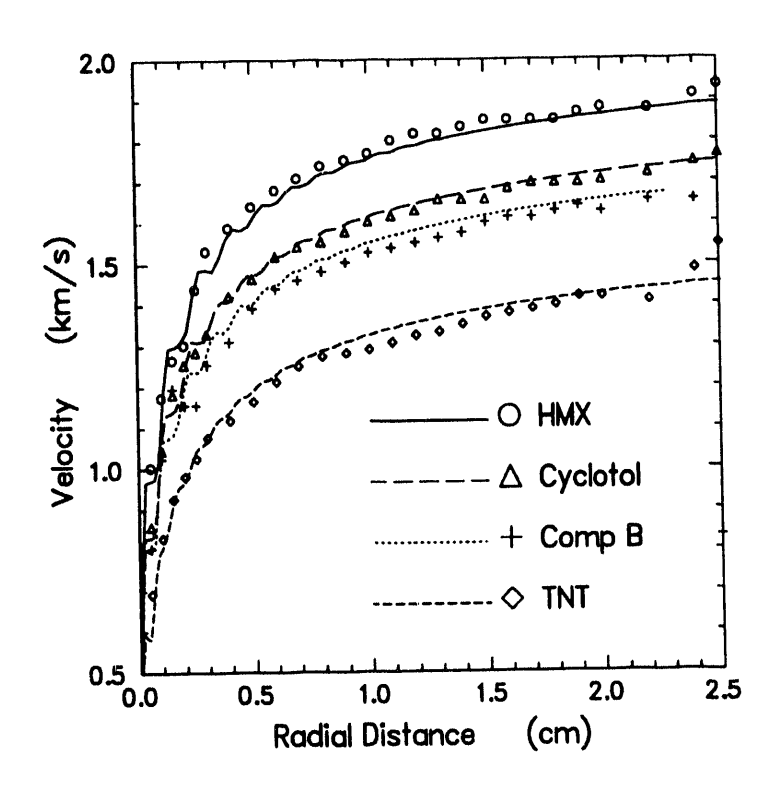


Fig. 7. Cylinder test results for RDX-TNT mixtures. Experimental data are from Ref. [1].

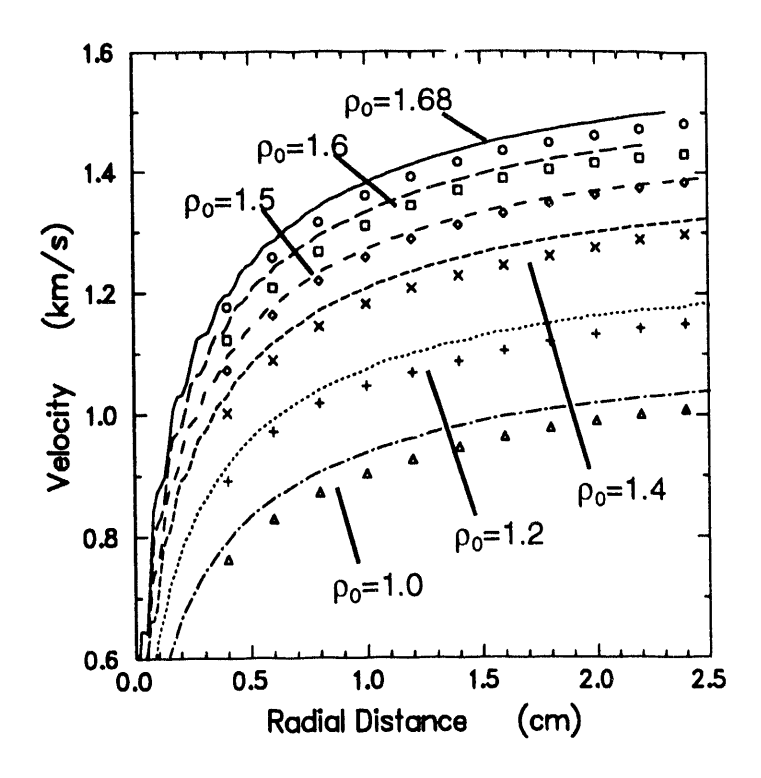


Fig. 8. Cylinder test results for HNS at various loading densities. Experimental data are from Ref. [27].

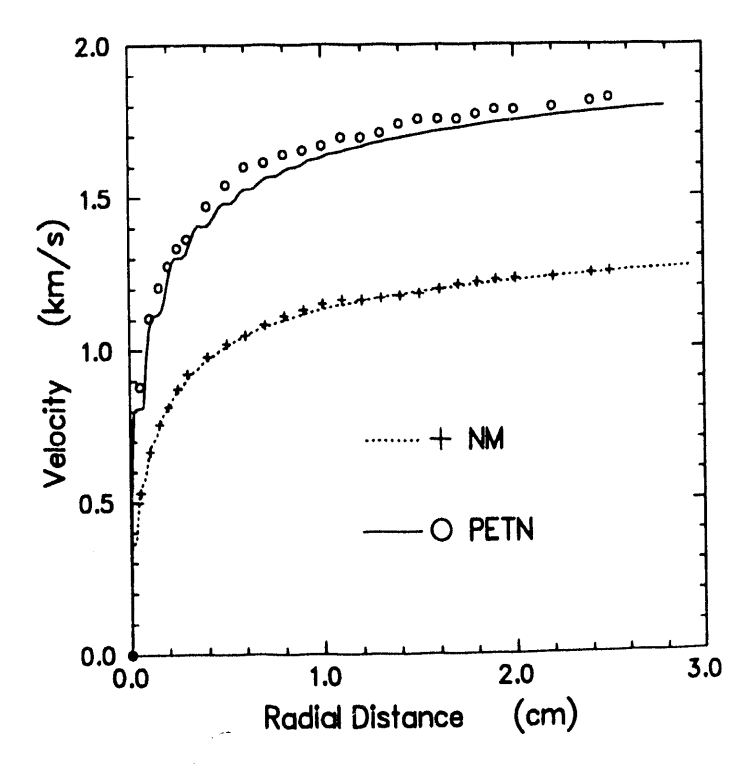


Fig. 9. Cylinder test results for PETN and NM. Experimental data are from Ref. [1].

The cylinder test results for PETN and NM are displayed in Fig. 9. The calculations are also in very good agreement with the measurements [1] for these two cases.

Figure 10 shows the velocity vs. radius curves for both 1-in [16] and 2-in [39] cylinder tests of the TATB-based explosive, PBX-9502. (The wall thickness was 0.26 cm in both cases.) The calculated curves have the correct shape but lie above the experimental ones by ~6% and ~3% for the 1-in and 2-in tests, respectively. These discrepancies are consistent with the results for the detonation velocity and are larger than those obtained for the other explosives studied.

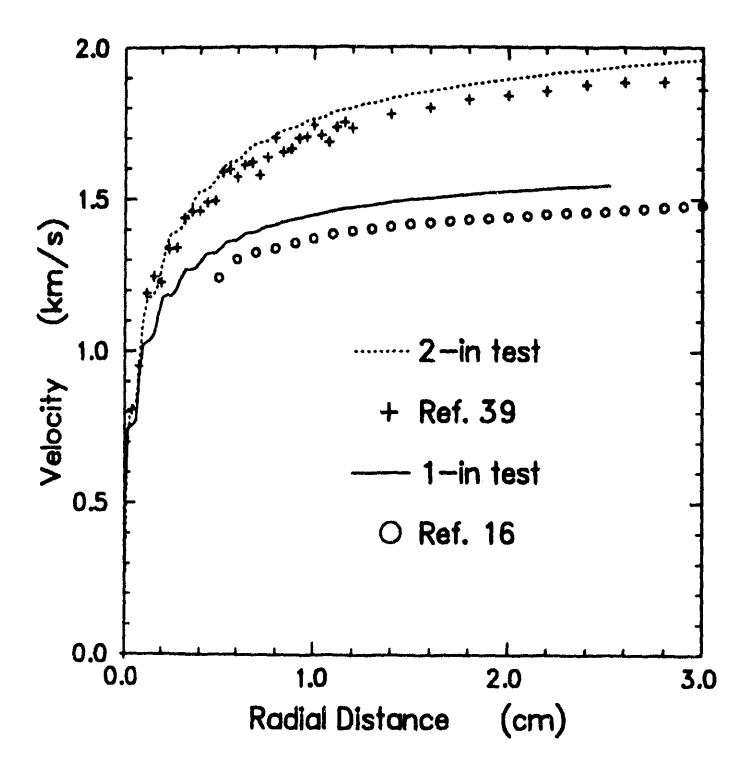


Fig. 10. 1-in and 2-in cylinder test results for PBX9502.

As noted in Sec. 3.1, TATB-based explosives exhibit nonideal behavior in that the infinite diameter detonation velocity is not attained for charge diameters as large as 13 cm [23][24]. Nonideal behavior has also been seen in interface velocity and plate-push experiments on TATB explosives [40][41][42]. The velocity (or energy) imparted to the target by the explosive is observed to increase with the length of the charge. Tang [42] has shown that these data can be reproduced using a two-step reactive burn model; about 85% of the energy is released by a fast reaction, which takes 20 ns, while the rest of the energy is released by a slow reaction that requires an additional 240 ns. The total reaction zone length in Tang's model is about 0.2 cm, which is comparable to the wall thickness in the cylinder tests. The slow reaction must also play a role in determining the effect of diameter on the detonation velocity and cylinder wall velocity.

In principle, the effects of nonideal behavior can be treated through the reactive burn model. However, the HVRB model used here was calibrated using shock initiation data and

does not include any slow reaction. Therefore it gives only a rough description of the reaction zone. Preliminary calculations show that adding a slow reaction to the HVRB model does improve the cylinder test predictions. However, a complete study of this problem is beyond the scope of the present work.

A summary of all the cylinder test calculations is given in Table 3. The wall velocities are tabulated at radial displacements of 0.6, 1.25, and 1.9 cm, corresponding to volumetric expansions of ~2, ~4, and ~7, respectively. In addition to the explosives shown in Figs. 2 through 10, the table gives results for 11 explosives considered in Ref. [10], for which detailed velocity histories were not available to the present authors. Five of these - TATB, TNGU, NNE, HNO₃#1, and HNO₃#2 - are CHNO compositions. Three of them - BTF, HNB, and TNM - are CNO compositions. The other three - RX-23-AA, RX-23-AB, and RX-23-AC - are HNO compositions.

As shown in Table 3, the average difference between the calculated and experimental cylinder wall velocities at 0.6-cm expansion is only 0.2%, with a standard deviation of 2.8%. The results are essentially the same for the 1.25- and 1.90-cm expansions, showing that the shapes of the velocity vs. radius curves are predicted correctly. As noted above, the TATB-based explosives show larger deviations than the others, probably because of non-ideal behavior. HNB, low density HNS, and RX-23-AA also show deviations of ~4%, somewhat larger than average.

3.3 Plate Acceleration Tests

Lee, et al. [21] studied the motion of metal walls driven by the HMX-based explosive LX14 in flat plate geometries as well as in cylinder tests. They found that the JWL EOS parameters previously derived from cylinder tests did not give satisfactory results when used to calculate the flat plate tests. They concluded that the cylinder test measurements sample the detonation product EOS at densities $\rho < \rho_0$ (where ρ_0 is the initial explosive density), while the flat plate tests are also sensitive to the EOS at higher compressions, $\rho_0 < \rho < \rho_C$. They also found that higher plate velocities were obtained for thinner plates, indicating the influence of the reaction zone. By reducing the CJ pressure from 37 GPa to 36 GPa, they derived a new set of JWL parameters that fit both the cylinder test data and the plate data for thicknesses greater than 0.05 cm. However, they were not able to fit all of the thin plate data, even using a reactive burn model.

Figure 11 compares the velocity history calculated using the PANDA EOS with two Fabry-Perot records for a copper plate of thickness 0.0526 cm, driven by a 1.995-cm thickness of explosive. The predictions agree very well with the measurements, even though the PANDA EOS has a CJ pressure of only 33.8 GPa, in contrast to the value of 36 GPa obtained in Ref. [21]. The CTH input file for this problem is given in Appendix C. As discussed below, the results for this test are much less sensitive to the reactive burn model than for the tests using thinner plates. This problem was found to be rather sensitive to zoning; in order to obtain good resolution, a zone size of 0.001 cm was used in the vicinity of the copper plate, while graded zoning was used in the outer parts of the computational mesh.

TABLE 3: Summary of copper cylinder w ...l velocity calculations. All calculations were for 1-in diameter, 0.26-cm wall thickness, except where indicated. R-R₀ is the cylinder radius minus the initial radius.

	Initial	Wall Velocity (km/s)						
Explosive	Density	$R-R_0=0.6 \text{ cm}$		$R-R_0=1.25 \text{ cm}$		$R-R_0=1.9 \text{ cm}$		Refs.
	(g/cm^3)	expt.	calc.	expt.	calc.	expt.	calc.	
BTF	1.852	1.605	1.634	1.755	1.770	1.835	1.839	[10]
Comp B (Gr. A)	1.717	1.439	1.447	1.556	1.588	1.640	1.648	[1]
Cyclotol (77/23)	1.754	1.516	1.519	1.640	1.652	1.695	1.714	[1]
HMX	1.894	1.650	1.649	1.820	1.800	1.883	1.860	[1][10]
HMX	1.188	1.173	1.149	1.314	1.287	1.384	1.348	[10]
HNB ³	1.965	1.700	1.600	1.880	1.808	1.955	1.885	[10]
HNO ₂ #1	1.542	1.295	1.279	-	1.452	-	1.531	[10]
HNO ₃ #2	1.560	1.210	1.245	1.370	1.400	-	1.470	[10]
HNS	1.681	1.255	1.283	1.385	1.416	1.458	1.476	[27]
HNS	1.402	1.081	1.116	1.207	1.239	1.266	1.294	[27]
HNS	1.001	0.817	0.861	0.931	0.967	0.981	1.013	[27]
LX09	1.840	1.649	1.595	1.758	1.743	1.828	1.804	[22]
LX14 (X-0282)	1.835	1.587	1.584	1.713	1.726	1.777	1.787	[16][22]
LX14 (2-in)	1.835	1.963	1.911	2.152	2.140	2.260	2.249	[21]
NM^b	1.13	1.045	1.047	1.180	1.165	1.230	1.219	[1][10]
NNE ^b	1.034	0.836	0.859	0.935	0.960	0.990	1.010	[10]
PBX9011	1.770	1.504	1.508	1.633	1.637	1.681	1.697	[1]
PBX9404	1.840	1.603	1.588	1.734	1.737	1.793	1.796	[16][22]
PBX9501	1.834	1.570	1.590	1.707	1.734	1.776	1.795	[16]
PBX9502	1.894	1.301	1.364	1.398	1.475	1.435	1.520	[16]
PBX9502 (2-in)	1.880	1.565	1.624	1.759	1.809	1.827	1.885	[39]
PETN	1.765	1.560	1.524	1.705	1.670	1.790	1.739	[1][10]
PETN	1.498	1.355	1.306	1.510	1.465	1.590	1.538	[10]
PETN	1.266	1.156	1.145	1.304	1.295	1.382	1.364	[10]
RX-23-AA ^b	1.424	1.320	1.299	1.473	1.401	1.520	1.446	[10]
RX-23-AB	1.356	1.080	1.052	1.180	1.145	1.210	1.184	[10]
RX-23-AC	1.136	1.075	1.072	1.170	1.162	1.220	1.195	[10]
TATB ^b	1.83	1.300	1.362	1.403	1.480	1.453	1.530	[10]
TNGU	1.885	1.600	1.558	1.750	1.703	1.825	1.775	[10]
TNM	1.650	1.000	1.019	1.095	1.103	1.130	1.135	[10]
TNT^b	1.632	1.210	1.231	1.355	1.362	1.410	1.420	[1][10]
average difference	e (calc./expt	11)	+0.2%		+0.3%		0.0%	
standard, deviation	n		2.8%		2.6%		2.6%	

^a Experimental data are for 3/4-in diameter, scaled to 1-in [10].

^b Experimental data are for 2-in diameter, scaled to 1-in [10].

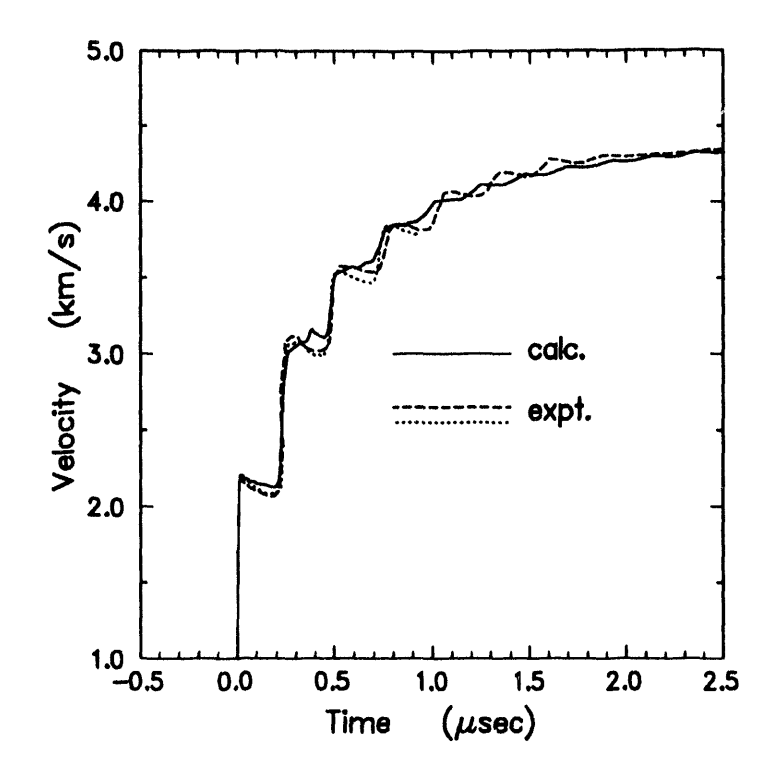


Fig. 11. LX14 flat plate tests #9633 and 9634 of Ref. [21]. HE thickness - 1.995 cm, copper thickness - 0.0526 cm, zone size - 0.001 cm in vicinity of copper plate.

Analysis of the flat plate experiments illustrates the difficulty of obtaining the CJ pressure from experimental data. The plate motion at early times is determined primarily by the leading part of the detonation wave (including the reaction zone), while the motion at later times depends upon the detonation product expansion and also the thickness of the explosive. Figure 12 shows the initial acceleration of the copper plate (the first plateau in the velocity time history), for the 19 experiments reported in Ref. [21]. It can be seen that the initial velocity is ~2.1±0.1 km/s, independent of thickness, for thicknesses greater than 0.01 cm, indicating that the reaction zone has a relatively small effect. However, the higher velocity obtained for a thickness of 0.0025 cm suggests the presence of a von Neumann spike. The ratio R of the copper thickness to the explosive thickness is also indicated. There is no correlation with explosive thickness within the scatter in the data.

The initial plate velocity can be estimated by impedance matching, using the diagram shown in Fig. 13. The Hugoniot for the explosive detonation products is shown by the solid line, with the CJ state denoted as point A. The initial shock state in the copper plate, point B, corresponds to the intersection of the copper Hugoniot with the second shock Hugoniot for the detonation products. The free surface velocity of the copper plate corresponds to zero pressure on the copper release curve, point C. Using the PANDA EOS for the detonation products and the Mie-Grüneisen EOS for copper, the velocity obtained is 2.14 km/s, in good agreement with the experimental data, as shown by the dotted line in Fig. 12. This calculation is only approximate because it ignores the effects of the Taylor wave and the reaction zone. However, it shows that the plate motion is determined not

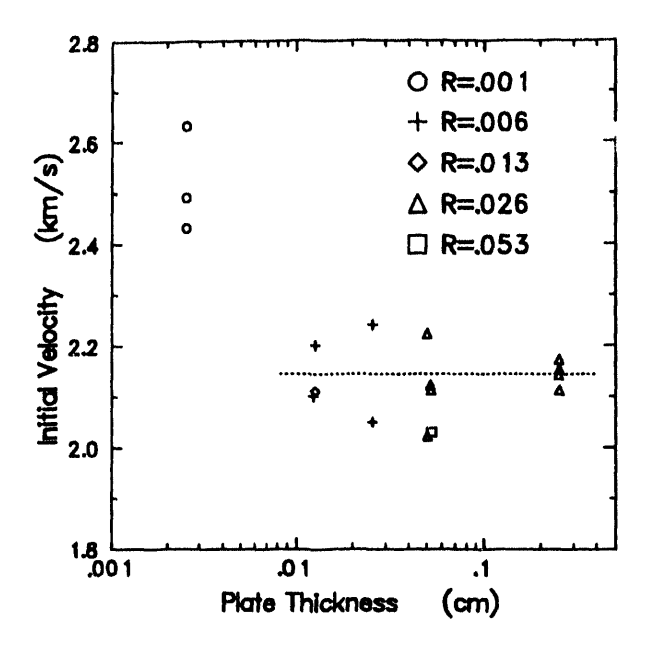


Fig. 12. Initial acceleration of copper plate for experiments reported in Ref. [21]. R is the ratio of the copper plate thickness to the thickness of the explosive. The dotted line shows a velocity of 2.14 km/s, computed as described in the text.

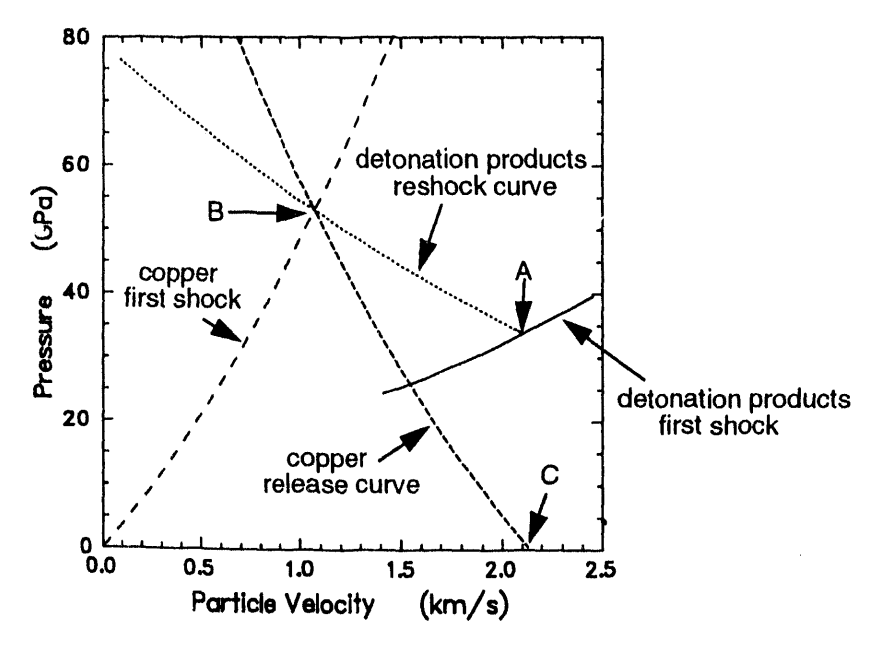


Fig. 13. Impedance matching diagram for interaction of copper plate with LX14 explosive. Point A is the CJ state for explosive, B is shock state in the copper and reshock state in detonation products, C is release state in the copper.

only by the CJ state, but also by the reshock behavior of the detonation products. That fact explains why two EOS having quite different CJ pressures can give similar results for the plate motion.

A reasonable description of the reaction zone is needed for the experiments involving very thin plates. In the HVRB model, the parameters that have the greatest effect on the reaction zone are the EOS for the unreacted explosive (which determines the von Neumann spike pressure) and the constant P_r in Eq. (4) (which determines the overall zone length). However, the HVRB model was developed primarily for modeling shock initiation phenomena, and Eqs. (1)-(4) were not derived to give an accurate description of the reaction zone. The values obtained by calibrating the model to shock initiation data, as described in Sec. 2.3, do not give satisfactory results when extrapolated into the present regime, overestimating the effects of the reaction zone on the plate velocity. Since there are no independent measurements that can be used to determine the necessary parameters, the value of P_r was adjusted to match the initial velocity of a 0.00254 cm copper plate, while the other burn parameters were unchanged from their original values. The adjusted value of P_r (about 1/5 of the original value) was used in the calculation shown in Fig. 11; the velocities obtained using the original value of P_r were ~3% higher.

Figure 14 compares the calculated curves with experimental data for a 0.00254 cm copper plate, using the adjusted value of P_r . The theoretical results agree with measurements at both early times, as expected, and also at late times, where the velocity depends on the detonation product expansion and the explosive thickness. The results for an intermediate copper thickness of 0.0126 cm are shown in Fig. 15. The calculated velocities are in satisfactory agreement with experiment, given the scatter in the data (data for the other tests at this thickness show variations of $\sim 4\%$ [21]).

The fact that the PANDA model gives good agreement with both flat plate and cylinder tests, which sample different regions of the EOS surface, is further evidence of its generality. It may be possible to improve the calculations for thin plates by refining the reactive burn model.

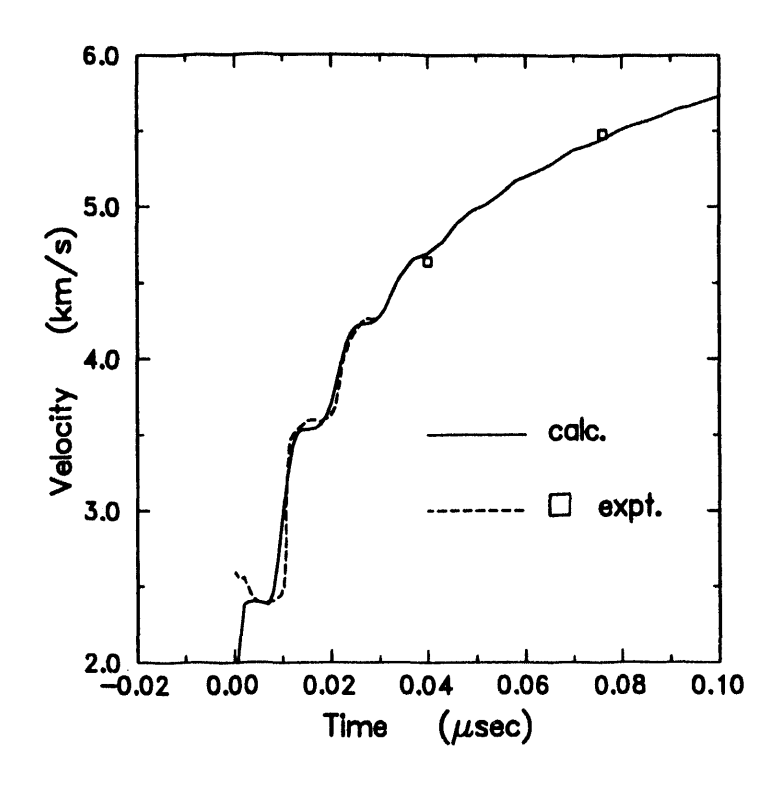


Fig. 14. LX14 flat plate test #9643 of Ref. [21]. HE thickness - 2.558 cm, copper thickness - 0.00254 cm, zone size - 0.0002 cm in vicinity of copper plate.

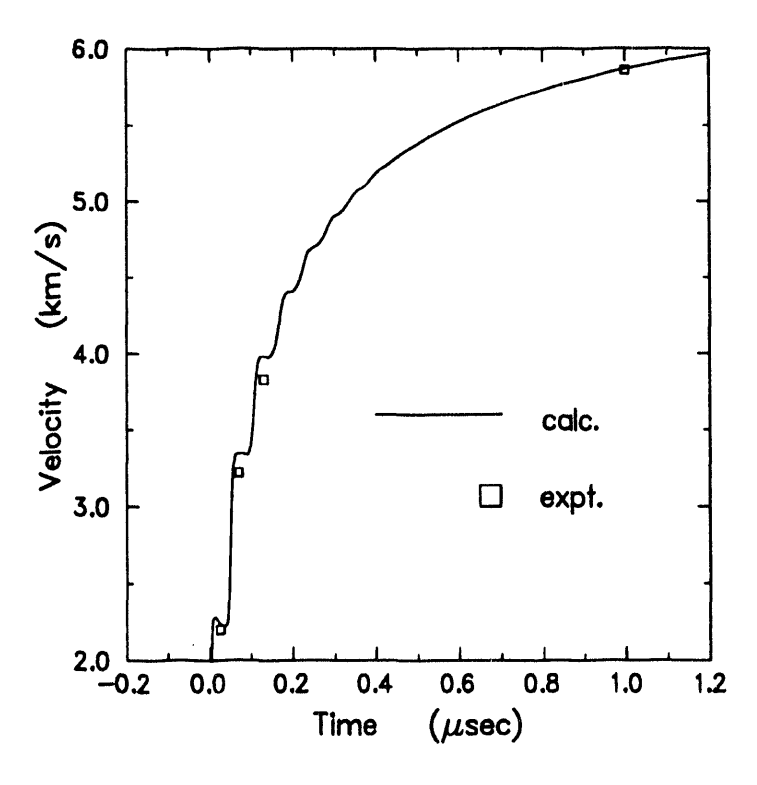


Fig. 15. LX14 flat plate test #9526 of Ref. [21]. HE thickness - 1.997 cm, copper thickness - 0.0126 cm, zone size - 0.0005 cm in vicinity of copper plate.

4. Summary and Conclusions

Accurate EOS for explosive detor ation products, and the means for using these EOS in hydrocode calculations, are needed in many practical applications which involve the modeling of explosives and other energetic materials. Until recently, analysts have often had to rely on simple analytical EOS formulas for the study of complicated problems. A sophisticated tabular EOS package and reactive burn model [20], which was recently developed for the CTH hydrocode, offers a more realistic treatment of explosives than was previously available. This capability has been used in the present study.

The present work and previous studies [7][8] have demonstrated that the PANDA code can be used to construct accurate a priori EOS for the detonation products of CHNO explosives. The PANDA EOS are in very good agreement with experimental detonation properties, overdriven shock data, cylinder test expansion meaurements and plate push tests. Hence one advantage of the PANDA code is that it provides a way to predict the EOS for new compositions. By contrast, the analytic JWL formula must be fit to experimental data for each explosive.

It is equally important to recognize that the PANDA code predicts a very different EOS surface from the one obtained with the JWL formula, even though the two models may give comparable results for cylinder tests. Because the PANDA model incorporates the fundamental physics and chemistry of the problem, it is reliable over a wide range of conditions. By contrast, it is well known that JWL parameters obtained from cylinder tests often give poor results in plate push tests, in overdriven shock experiments, and in other problems outside the region of calibration [11][21]. These difficulties arise because of the simplicity of the JWL expression, i.e. the use of a constant specific heat and Grüneisen parameter. The availability of a tabular EOS package eliminates the need to fit the EOS to an analytic function.

Reactive burn phenomena have been relegated to a secondary role in the present study, but certain points should be noted. First, the predicted detonation properties and cylinder wall velocities for TATB-based explosives show larger discrepancies with experiment than do the other explosives. Some of these discrepancies are clearly due to nonideal behavior, which has been observed in the effect of diameter on detonation velocity [23][24] and the effect of charge length on the energy imparted to a target [40]-[42]. Second, the velocity histories of thin plates accelerated by LX14 also show effects due to the reaction zone [21]. These problems show that the detonation product EOS can be separated from reactive burn phenomena only to a first approximation. However, a full analysis of reactive effects would have required more time than could be devoted to the present study.

References

- [1] E. L. Lee, H. C. Hornig, and J. W. Kury, "Adiabatic Expansion of High Explosive Detonation Products," report UCRL-50422, Lawrence Radiation Laboratory, Livermore, CA, May 2, 1968.
- [2] C. L. Mader, Numerical Modeling of Detonations (University of California, Berkeley, 1979).
- [3] M. Finger, E. Lee, F. H. Helm, B. Hayes, H. Hornig, R. McGuire, and M. Kahara, "The Effect of Elemental Composition on the Detonation Behavior of Explosives," in Proceedings of the Sixth Symposium (International) on Detonation, edited by D. J. Edwards, ACR-221 (Office of Naval Research, Department of the Navy, 1976), pp. 710-722.
- [4] M. Cowperthwaite and W. H. Zwisler, "The JCZ Equations of State for Detonation Products and Their Incorporation into the TIGER Code," in Proceedings of the Sixth Symposium (International) on Detonation, edited by D. J. Edwards, ACR-221 (Office of Naval Research, Department of the Navy, 1976), pp. 162-170.
- [5] R. Chirat and G. Pittion-Rossillon, "A New Equation of State for Detonation Products," J. Chem. Phys. 74, 4634-4642 (1981).
- [6] F. H. Ree, "Postdetonation Behavior of Condensed High Explosives by Modern Methods of Statistical Mechanics," in Proceedings of the Seventh Symposium (International) on Detonation, edited by J. M. Short, NSWL MP 82-334 (Naval Surface Weapons Center, White Oak, MD, 1981), pp. 646-660.
- [7] G. I. Kerley, "Theoretical Equations of State for the Detonation Properties of Explosives," in Proceedings of the Eighth Symposium (International) on Detonation, edited by J. M. Short, NSWL MP 86-194 (Naval Surface Weapons Center, White Oak, MD, 1986), pp. 540-547.
- [8] G. I. Kerley, "Theoretical Model of Explosive Detonation Products: Tests and Sensitivity Studies," in Proceedings of the Ninth Symposium (International) on Detonation, edited by W. J. Morat, OCNR 113291-7 (Office of the Chief of Naval Research, 1990), pp. 443-451.
- [9] M. L. Hobbs and M. R. Baer, "Nonideal Thermodynamic Calculations Using a Large Product Species Data Base," Sandia National Laboratories report SAND92-0482, 1992.
- [10] P. C. Souers and J. W. Kury, "Comparison of Cylinder Data and Code Calculations for Homogeneous Explosives," report UCRL-JC-110661, Lawrence Livermore National Laboratory, Livermore, CA, May 1992.

- [11] E. L. Lee, M. Van Thiel, L. G. Green, and A. Mitchell, "Detonation Product EOS: The Region Above Chapman-Jouget Pressure," Proceedings of the APS 1983 Topical Conference on Shock Waves in Condensed Matter, edited by J. R. Asay, R. A. Graham, and G. K. Straub (North-Holland, New York, 1984) p. 617.
- [12] G. I. Kerley, "User's Manual for PANDA II: A Computer Code for Calculating Equations of State," Sandia National Laboratories report SAND88-2291, 1991.
- [13] G. I. Kerley, "A Model for the Calculation of Thermodynamic Properties of a Fluid Using Hard-Sphere Perturbation Theory and the Zero-Kelvin Isotherm of the Solid," in Molecular Based Study of Fluids, edited by J. M. Haile and G. A. Mansoori (Am. Chem. Soc., Washington, DC., 1983) pp 107-138.
- [14] G. I. Kerley, "Equations of State and Gas-Gas Phase Separation in Soft Sphere Mixtures," J. Chem. Phys. 91, 1204-1210 (1989).
- [15] B. M. Dobratz and P. C. Crawford, "LLNL Explosives Handbook," Lawrence Livermore National Laboratory report UCRL-52997, January 1985.
- [16] T. R. Gibbs and A. Populato, LASL Explosive Property Data (University of California, Berkeley, 1980).
- [17] J. M. McGlaun, F. J. Ziegler, S. L. Thompson, L. N. Kmetyk, and M. G. Elrick, "CTH User's Manual and Input Instructions," Sandia National Laboratories report SAND88-0523, April 1988.
- [18] E. S. Hertel, Jr., "A Comparison of the CTH Hydrodynamics Code With Experimental Data," Sandia National Laboratories report SAND92-1879, September 1992.
- [19] G. I. Kerley, "CTH Reference Manual: The Equation of State Package," Sandia National Laboratories report SAND91-0344, 1991.
- [20] G. I. Kerley, "CTH Equation of State Package: Porosity and Reactive Burn Models," Sandia National Laboratories report SAND92-0553, 1992.
- [21] E. Lee, D. Breithaupt, C. McMillan, N. Parker, J. Kury, C. Tarver, W. Quirk, and J. Walton, "The Motion of Thin Metal Walls and The Equation of State of Detonation Products," in Proceedings of the Eighth Symposium (International) on Detonation, edited by J. M. Short, NSWL MP 86-194 (Naval Surface Weapons Center, White Oak, MD, 1986), pp. 613-624.
- [22] E. L. Lee, F. H. Helm, M. Finger, and J. R. Walton, "Equations of State for Detonation Products of High Energy PBX Explosives," report UCID-17540, Lawrence Livermore Laboratory, Livermore, CA, Aug. 1, 1977.
- [23] A. W. Campbell, "Diameter Effect and Failure Diameter of a TATB-Based Explosive," Propellants, Explosives, Pyrotechnics 9, 183-187 (1984).

- [24] C. D. Hutchinson, G. C. W. Foan, H. R. Lawn, and A. G. Jones, "Initiation and Detonation Properties of the Insensitive High Explosive TATB/Kel-F 800 95/5," in Proceedings of the Ninth Symposium (International) on Detonation, edited by W. J. Morat, OCNR 113291-7 (Office of the Chief of Naval Research, 1990), pp. 123-132.
- [25] K. K. Shvedov, "Determination of the Chapman-Jouguet Parameters in the Detonation of Condensed Explosives," Combustion, Explosives, and Shock Waves 23, 464-474 (1987).
- [26] D. J. Steinberg, "Comparison of Experimental Data on Detonation Velocity and Chapman-Jouguet Pressure vs. Initial HE Density With Predictions From Ree's Model Equation of State," in Proceedings of the Eighth Symposium (International) on Detonation, edited by J. M. Short, NSWL MP 86-194 (Naval Surface Weapons Center, White Oak, MD, 1986), pp. 513-520.
- [27] P. E. Kramer, "HNS Cylinder Tests," Mason and Hanger-Silas Mason report MH-SMP-75-17, 1975.
- [28] A. W. Campbell and R. Engelke, "The Diameter Effect in High-Density Heterogeneous Explosives," in Proceedings of the Sixth Symposium (International) on Detonation, edited by D. J. Edwards, ACR-221 (Office of Naval Research, Department of the Navy, 1976), pp 642-652.
- [29] W. C. Davis and J. B. Ramsay, "Detonation Pressures of PBX-9404, Composition B, PBX-9502, and Nitromethane," in Proceedings of the Seventh Symposium (International) on Detonation, edited by J. M. Short, NSWL MP 82-334 (Naval Surface Weapons Center, White Oak, MD, 1981), pp. 531-539.
- [30] H. C. Hornig, E. L. Lee, M. Finger, and J. E. Kurrle, "Equation of State of Detonation Products," in Proceedings of the Fifth Symposium (International) on Detonation, edited by D. J. Edwards, ACR-184 (Office of Naval Research, Department of the Navy, 1970), pp. 503-511; the detonation pressure for the highest density includes a 6% correction by L. Green, personal communication, 1984.
- [31] M. J. Urizar, E. James, Jr., and L. C. Smith, "Detonation Velocity of Pressed TNT," Phys. Fluids 4, 262-274 (1961).
- [32] M. J. Kamlet and C. Dickenson, "Chemistry of Detonations. III. Evaluation of the Simplified Calculational Method for Chapman-Jouget Detonation Pressures on the Basis of Available Experimental Information," J. Chem. Phys. 48, 43-50 (1968).
- [33] I. M. Voskoboinikov, and A. Ya. Apin, "Measurement of Detonation Front Temperatures of Explosives," Dokl. Akad. Nauk SSSR 130, 805 (1960).
- [34] P. A. Urtiew, "Brightness Temperature of Detonation Wave in Liquid Explosives," Acta Astronautica 3, 555-566 (1976).

- [35] Y. Kato, N. Mori, H. Sakai, K. Tanaka, T. Sakurai, and T. Hikita, "Detonation Temperature of Nitromethane and Some Solid High Explosives," in Proceedings of the Eighth Symposium (International) on Detonation, edited by J. M. Short, NSWL MP 86-194 (Naval Surface Weapons Center, White Oak, MD, 1986), pp. 558-566. Also see references cited for nitromethane.
- [36] He Xianchu, Han Chengbung, and Kang Shufong, "The Measurement of Detonation Temperature of Condensed Explosives With Two Colour-Optical Fiber Pyrometer," in Proceedings of the Eighth Symposium (International) on Detonation, edited by J. M. Short, NSWL MP 86-194 (Naval Surface Weapons Center, White Oak, MD, 1986), pp. 567-574. Also see references cited for nitromethane, TNT, and PETN.
- [37] Y. Kato, N. Mori, H. Sakai, T. Sakurai, and T. Hikita, "Detonation Temperature of Some Liquid and Solid Explosives," in Proceedings of the Ninth Symposium (International) on Detonation, edited by W. J. Morat, OCNR 113291-7 (Office of the Chief of Naval Research, 1990), pp. 939-946.
- [38] S. Huisheng, H. Chengbang, K. Shufang, and H. Lihong, "The Studying of Detonation Temperature of Solid High Explosives," in Proceedings of the Ninth Symposium (International) on Detonation, edited by W. J. Morat, OCNR 113291-7 (Office of the Chief of Naval Research, 1990), pp. 947-952.
- [39] E. Baker, personal communication, 1992.
- [40] W. L. Seitz, H. L. Stacy, and J. Wackerle, "Detonation Reaction Zone Studies on TATB Explosives," in Proceedings of the Eighth Symposium (International) on Detonation, edited by J. M. Short, NSWL MP 86-194 (Naval Surface Weapons Center, White Oak, MD, 1986), pp. 123-132.
- [41] W. L. Seitz, H. L. Stacy, R. Engelke, P. K. Tang, and J. Wackerle, "Detonation Reaction-Zone Structure of PBX 9502," in Proceedings of the Ninth Symposium (International) on Detonation, edited by W. J. Morat, OCNR 113291-7 (Office of the Chief of Naval Research, 1990), pp. 657-669.
- [42] P. K. Tang, "Modeling Hydrodynamic Behaviors in Detonation," Propellants, Explosives, Pyrotechnics 16, 240-244 (1991).
- [43] S. A. Silling, "CTH Reference Manual: Viscoplastic Models," Sandia National Laboratories report SAND91-02923, 1991.
- [44] P. A. Taylor, "CTH Reference Manual: The Steinberg-Guinan-Lund Viscoplastic Model," Sandia National Laboratories report SAND92-0716, 1992.

Appendix A

PANDA Input File for PBX9404

```
06/18/93 - EOS for detonation products of PBX-9404.
! PBX-9404 is 94% HMX, 3% NC, 3% CEF by weight.
! Formula - c[1.40]h[2.75]n[2.57]o[2.69]cl[.03]p[.01] (100 g of
    explosive) - the cl and p are ignored in this setup.
    heat of formation (298K) = 0.00331 (Dobratz and Crawford)
1
!
! Energy zero of EOS tables is assumed to give zero enthalpy for
! elements in their standard states at 1 atm and 298K. Energy zero
! for table is unreacted explosive at 298K.
! htf is (-) heat of formation,
! mc, mh2, mn2, and mo2 are moles of c, h2, n2, and o2.
sym htf=-.00331 mc=1.40 mh2=1.375 mn2=1.285 mo2=1.345
mod mix ezro=htf
                      ! carbon dioxide
c[1]o[2]
 matid=201 name=co2 file=hesps eshift=-9.1552
                      ! molecular nitrogen
 matid=202 name=n2 file=hesps eshift=-.30900 moles=mn2
                      ! water
h[2]o[1]
 matid=203 name=h2o file=hesps eshift=-13.971
                      ! carbon monoxide
c[1]o[1]
 matid=204 name=co file=hesps eshift=-4.2551
c[1]h[4]
                      ! methane
 matid=205 name=ch4 file=hesps eshift=-5.2897
                      ! ammonia
n[1]h[3]
 matid=206 name=nh3 file=hesps eshift=-3.2789
                      ! molecular hydrogen
 matid=207 name=h2 file=hesps eshift=-4.1866 moles=mh2
                      ! molecular oxygen
0[2]
 matid=208 name=o2 file=hesps eshift=-.27085 moles=mo2
                      ! nitric oxide
n[1]o[1]
 matid=209 name=no file=hesps eshift=2.7206
h[2]c[1]o[2]
                      ! formic acid
 matid=301 name=hcooh file=hesps eshift=-8.4598
                      ! graphite
c[1]
 matid=213 name=grp ptyp=.01 file=hesps eshift=59.157 moles=mc
c[1]
                      ! fluid carbon
 matid=210 name=clq ptyp=.01 file=hesps eshift=59.157
                     ! diamond
c[1]
  matid=214 name=dia ptyp=.01 file=hesps eshift=60.057
```

```
n[1]
                         ! atomic nitrogen
  matid=102 name=n1 file=hesps eshift=33.294
                         ! atomic oxygen
0[1]
 matid=108 name=o1 file=hesps eshift=15.172
                         ! atomic hydrogen
h[1]
 matid=107 name=h1 file=hesps eshift=210.19
! Compute CJ state
cj mix
1.84
! Make EOS table - use set bas command to find FZ and FW
set bas
c[1.40]h[2.75]n[2.57]o[2.69] ! cl[.03]p[.01] - ignored
isot mix 3.1635 3.1647 20 1 298 0 1 1
slib mix
201
51.320 99.996 67.280 298 3.16
301
0 0 1 1
.01 .1 5 2
.1 5 45 2
298 1000 2 1
1.e3 1.e4 24 2
298 .29
8211 061893 b8211 a8211
! Read table back in and compute CJ properties
mod sol tab=1
8211 b8211
cj sol
1.84 0 0
end
```

Appendix B

CTH Input File for PBX9404 Cylinder Test

```
**************
               CTH Calculation of PBX9404 Cylinder Test
                             07/28/93
  1 in diameter stick of explosive enclosed in 0.26 cm thick Cu tube.
  15 cm length of explosive, cylinder expansion studied near 8 cm.
   - X-Mesh: uniform 0.02 cm zones out to 4.0 cm (13 zones in Cu),
     then graded region out to 6.0 cm.
   - Y-Mesh: uniform 0.05 cm zones from 5.0 to 10.0 cm, graded zones
     at beginning and end of stick.
   - Histories for recording cylinder expansion at 7, 8, and 9 cm, at
     surface of Cu wall. Histories for recording of arrival times at
     7, 8, and 9 cm, along cylinder axis.
   - Uses tabular EOS for detonation products of explosive.
   - Uses HVRB model to propagate detonation wave. Explosive is
     initiated by a 1.3 cm booster.
***************
*eor* genin - CTHGEN input
* Title record
PBX9404 Cylinder Test - Panda EOS, HVRB burn
* Control block
CONTROL
 MMP
ENDCONTROL
* Set up geometry and mesh
MESH
 BLOCK 1 GEOM=2DC TYPE=E
   X0 0.0
     X1 W=4.0 DXF=0.02 DXL=0.02
     X2 W=2.0 DXF=0.02 DXL=0.07
   ENDX
   Y0 - 1.3
     Y1 W=1.3 DYF=0.25 DYL=0.20
     Y2 W=5.0 DYF=0.20 DYL=0.05
     Y3 W=5.0 DYF=0.05 DYL=0.05
     Y4 W=5.0 DYF=0.05 DYL=0.20
   ENDY
   XACT 0.0 1.5
   YACT -1.3 0.0
 ENDB
 ENDMESH
* Material insertion inputs
 INSERTION of MATERIAL
  BLOCK 1
```

```
PACKAGE BOOSTER
     MATERIAL 3
     INSERT BOX
       X1 0.0 X2 1.27
Y1 -15.0 Y2 0.0
     ENDINSERT
   ENDPACKAGE
   PACKAGE HE
     MATERIAL 2
     INSERT BOX
       X1 0.0 X2 1.27
                Y2 25.0
       Y1 -15.0
     ENDINSERT
   ENDPACKAGE
    PACKAGE COPPER CASE
     MATERIAL 1
     INSERT BOX
       X1 1.27 X2 1.53
       Y1 -15.0 Y2 25.0
      ENDINSERT
    ENDPACKAGE
  ENDBLOCK
ENDINSERTION
* EOS input set - new interface
EOS
* Copper - Mie-Gruneisen
 MAT1 MGRUN
       R0=8.94 CS=3.94E5 S=1.489 G0=1.99 CV=4.56E10
* PBX9404 Explosive - Panda EOS with HVRB model
 MAT2 SESAME EOS=8211 FEOS='sesame'
       RP=1.84 R0=1.873 CS=2.9E5 S=2.0 G0=1.0 CV=1.35E11
       TYP=2.0 PR=5.9E10 ZR=2.36 MR=1.5 PI=0.5E10
       RMAX=5.0 RMIN=0.1 TMAX=5.0 PT=1.0E13
* PBX9404 Explosive - JWL
 MAT3 JWL
       R0=1.84 AG=8.524 BG=0.1802 CG=0.01207
       R1=4.60 R2=1.30 WG=0.38 PCJ=0.370 DCJ=0.880
 ENDEOS
* HEBURN input set
 HEBURN
  MAT 3 D=8.80E5
    DL 0.0,-1.3 TO 1.5,-1.3 R=100.0 TIME=0.0
 ENDHE
* Elastic-plastic Input set
 EPDATA
  MATEP 1 YIELD=3.5E9 POISSON=0.35
  MIX 3
************************
 ENDE
*eor* cthin - CTH input
* Title record
PBX9404 Cylinder Test - Panda EOS, HVRB burn
* Control block
 CONTROL
```

Cylinder Test Predictions Using Panda EOS

```
TSTOP = 29.0E-6
 RDUMPF = 3600.
 CPSHIFT = 999.
 NTBAD 100000
ENDC
* Choose fluxing and interface options
  CON=1
  INT=HIGH
  NOFRAGMENT 1
  NOFRAGMENT 2
 ENDC
* First 3 tracers are near to OD of copper tube
* Second 3 tracers are near to cylinder axis
 TRACER
   ADD 1.48,7.0 to 1.48,9.0 N=3 FIXED=Y
   ADD 0.08,7.0 to 0.08,9.0 N=3
* Edit specifications
 EDIT
  SHORTT
    TIME=0.0 DT=5.0E-4
  ENDS
  LONGT
    TIME=0.0 DT=5.0E-4
   ENDL
   PLOTT
     TIME=0.0 DT=5.0E-6
   ENDP
   HISTT
     TIME=0.0 DT=5.0E-8
     HTRACER1
     HTRACER2
     HTRACER3
     HTRACER4
     HTRACER5
     HTRACER6
   ENDH
  ENDE
 * Define boundary conditions
  BOUNDARY
    BHY
         BXB = 0 , BXT = 1
         BYB = 1 , BYT = 1
       ENDB
     ENDH
   ENDB
  * Set minimum and maximum time steps
   MINDT
     TIME = 0. DT = 1.E-11
   ENDN
   MAXDT
     TIME = 0. DT = .01
```

Appendix B

```
ENDX
* Fracture input set
FRACTS
PRESSURE
PFRAC1 -0.3E10
PFRAC2 -5.0E6
PFRAC3 -5.0E6
PFMIX -0.3E10
PFVOID -0.3E10
ENDF
```

Appendix C

CTH Input File for LX14 Plate Acceleration Test

```
CTH Calculation of LX-14 Plate Experiment #9634
                                08/30/93
  Test data reported by Lee, et. al., 8th Det. Sym., pp 613-624.
  1.995 cm thickness of LX-14 accelerates 0.0526 cm Cu plate.
  Explosive initiated by using JWL/programmed burn in first 0.2 cm.
   - Mesh: Zones graded from 0.03 cm down to 0.001 cm for first 1.90
           cm, then 0.001 cm zones (53 zones in Cu) for 0.6 cm,
           then graded zones on outer part of mesh.
   - Panda EOS with HVRB for explosive.
*eor* genin - CTHGEN input
* Title record
PL9634 - /2.0 LX-14/->/.053 Cu/ Panda/HVRB
Control block
CONTROL
 MMP
* CHECKMESH
ENDCONTROL
* Set up geometry and mesh
MESH
 BLOCK 1 GEOM=1DR TYPE=E
   X0 0.0
     X1 W=1.90 DXF=0.030 DXL=0.001
     X2 W=0.60 DXF=0.001 DXL=0.001
     X3 W=0.50 DXF=0.001 DXL=0.010
   ENDX
   XACT -2.0 0.20
 ENDB
ENDMESH
* Material insertion inputs
INSERTION of MATERIAL
  BLOCK 1
    PACKAGE BOOSTER
      MATERIAL 3
      INSERT BOX
             0.0 X2 0.2
        X1
      ENDINSERT
    ENDPACKAGE
    PACKAGE HE
      MATERIAL 2
      INSERT BOX
        X1 0.2 X2 1.9954
```

ENDINSERT

```
ENDPACKAGE
    PACKAGE COPPER PLATE
      MATERIAL 1
      INSERT BOX
        X1 1.9954 X2 2.048
      ENDINSERT
    ENDPACKAGE
  ENDBLOCK
ENDINSERTION
* EOS input set - new interface
EOS
* Copper - Mie-Gruneisen
 MAT1 MGRUN
       R0=8.94 CS=3.94E5 S=1.489 G0=1.99 CV=4.56E10
* LX14 Explosive - Panda EOS with HVRB model
 MAT2 SESAME EOS=8231 FEOS='sesame'
       RP=1.835 R0=1.850 CS=2.9E5 S=2.0 G0=1.0 CV=1.35E11
       TYP=2.0 PR=1.7E10 ZR=2.36 MR=1.5 PI=0.5E10
       RMAX=5.0 RMIN=0.01 TMAX=5.0 PT=1.0E13
* LX-14 Explosive - JWL
 MAT3 JWL
       R0=1.835 AG=8.261 BG=0.1724 CG=0.01296
       R1=4.55 R2=1.32 WG=0.38 PCJ=0.370 DCJ=0.880
ENDEOS
* HEBURN input set
HEBURN
  MAT 3 D=8.80E5
    DP 0.0 R=100.0 TIME=0.0
ENDHE
* Elastic-plastic Input set
EPDATA
  MATEP 1 YIELD=3.5E9 POISSON=0.35
  MIX 3
ENDE
*eor* cthin - CTH input
* Title record
PL9634 - /2.0 LX-14/->/.053 Cu/ Panda/HVRB
* Restart instructions
* RESTART
* TIME=2.0E-6
* ENDR
* Control block
 CONTROL
  TSTOP = 5.0E-6
  RDUMPF = 3600.
 CPSHIFT = 999.
 NTBAD 100000
ENDC
* Choose fluxing and interface options
CONVCT
 CON=1
 ENDC
* Edit specifications
```

```
TRACER
  ADD 2.0455 to 2.0475 N=3
ENDT
EDIT
 SHORTT
   TIME=0.0 DT=5.0e-4
 ENDS
 LONGT
   TIME=0.0 DT=5.0e-4
 ENDL
 PLOTT
   TIME=0.0 DT=0.5e-6
 ENDP
 HISTT
   TIME=0.0 DT=5.E-8
   TIME=2.0E-6 DT=5.E-10
   HTRACER1
   HTRACER2
   HTRACER3
 ENDH
ENDE
* Define boundary conditions
BOUNDARY
  BHY
    BL 1
       BXB = 1 , BXT = 1
    ENDB
  ENDH
ENDB
* Set minimum and maximum time steps
 MINDT
   TIME = 0. DT = 1.E-11
 ENDN
 MAXDT
   TIME = 0. DT = .01
 ENDX

    Fracture input set

 FRACTS
   PRESSURE
   PFRAC1 -0.3E10
   PFRAC2 -0.3E10
   PFMIX -0.3E10
   PFVOID -0.3E10
 ENDF
```

External Distribution

Stanley Klein, M2/321 The Aerospace Corp. PO Box 92957 Los Angeles, CA 90009-2957

Eric Wong, M4/901 The Aerospace Corp. PO Box 92957 Los Angeles, CA 90009-2957

R. Blandford AFTAC/TT/CSS Suite 1450 1300 N. 17th St. Arlington, VA 22209

G. R. Johnson Alliant Techsystems Inc. 7225 Northland Dr. Brooklyn Park, MN 55428

Eric Peterson MN11-2720 Alliant Techsystems, Inc. 600 Second St., NE Hopkins, MN 55343

M. Alme
Alme and Associates
102 Stevens Forest Professional Center
9650 Santiago Road
Columbia, MD 21045

J. Walker Amparo Corporation P. O. Box 2687 Santa Fe, NM 87504

Frank Maestas
Principal Engineer
Applied Research Associates
4300 San Mateo Blvd.
Suite A220
Albuquerque, NM 87110

Richard Zernow Applied Research Associates 714 West Jefferson Ave. Suite 305 Lakewood, CO 80235

Howard Chung Argonne National Laboratory RE/331 9700 South Cass Avenue Argonne, IL 60439-4817

Ernest L. Baker Bldg 3022, SMCAR-AEE-WW U. S. Army ARDEC Picatinny Arsenal, NJ 07806-5000

U.S. Army Research Laboratory (5)
Aberdeen Proving Ground, MD 21005-5066
Attn: R. B. Frey
Attn: K. Kimsey, AMSRL-WT-TC
Attn: R. Lieb, SLCBR-IB-P
Attn: J. Starkenberg
Attn: J. Zukas, AMSRL-WT-TC

John Tipton U. S. Army Engineer Division HNDED-SY PO Box 1600 Huntsville, AL 35807

R. Rohani
U.S. Army Engineer Waterways Experiment
Station
Attn: CEWES-SD
3909 Halls Ferry Road
Vicksburg, MS 39180-6199

Shun-chin Chou Army Materials Technology Laboratory SLCMT-MRD Watertown, MA 02172-0001

George Snyder (2)
U. S. Army Missile Command
AMSMI-RD-ST-WF
Redstone, Arsenal, AL 35898-5247
Attn: J. Billingsley, G. Snyder

David Tenenbaum

U. S. Army Tank Automotive Command

RD&E Center

Survivability Division Mail Code MASTA-RSS Warren, MI 48397-5000

R. D. Everhart

Battelle Memorial Institute

505 King Ave.

Columbus, OH 43201-2693

Glen Salo

BDM Corporation 1801 Randolph Road SE

Albuquerque, NM 87106

Richard Bever

Bettis Atomic Power Laboratory Westinghouse Electric Company

Box 79

West Mifflin, PA 15122-0079

Steven Bishop

Belvoir RD&E Center

STRBE-NAA

Fort Belvoir, VA 22060-560

Kevin Housen (2), MS 87-60

The Boeing Company

PO Box 3999

Seattle, WA 98124

Attn: K. Housen, R. Schmidt

T. J. Ahrens

Seismological Laboratory

Division of Geological and Planetary Sciences

California Institute of Technology

Pasadena, CA 91125

S. Schuster

California Research & Technology

20943 Devonshire St.

Chatsworth, CA 94588

Dennis L. Orphal

California Research & Technology, Inc.

5117 Johnson Dr.

Pleasanton, CA 94588

Mark Majerus

California Research and Technology, Inc.

PO Box 2229

Princeton, NJ 08543-2229

Mark Smith

Aerophysics Branch

Calspan Corporation/AEDC Operations

MS 440

Arnold AFB, TN 37389

G. Lyles

CIA

6219 Lavell Ct.

Springfield VA 22152

John Walton

OSWR

CIA

Washington, DC 20505

N. W. Ashcroft

Laboratory of Atomic and Solid State Physics

Clark Hall

Cornell University

Ithaca, NY 14853

Carlos Marino

Industry, Science, and Technology Department

Cray Research Park 655 E. Lone Oak Dr.

Eagan, MN 55121

Stanley Willner

David Taylor Research Center

Mail Code 3510

Bethesda, MD 20084

Major Robert Kocher

Defense Advanced Research Projects Agency

3701 North Fairfax Drive

Arlington, VA 22203-1714

R. J. Lawrence DNA/SPSP

6801 Telegraph Rd.

Alexandria, VA 22310

Michael E. Giltrud DNA/SPSD 6801 Telegraph Rd. Alexandria, VA 22310

Randy Hanson Denver Research Institute University Park Denver, CO 80208

Brian Scott
EI Dupont de Demours and Company
Chestnut Run - CR702
Wilmington, DL 19898

William Flis DynaEast Corporation 3201 Arch Street Philadelphia, PA 19104

Randall Laviolette EG&G Idaho P.O. Box 1625 Idaho Falls, ID 83415-2208

Tien Chou EG&G Mound PO Box 3000 Miamisburg, OH 45343

Julius W. Enig Enig Associates, Inc. 11120 New Hampshire Ave., Suite 500 Silver Spring, MD 20904-2633

Kim Parnell Failure Analysis Associates, Inc. 149 Commonwealth Ave. P. O. Box 3015 Menlo Park, CA 94025

Vensen Wu FMC Corporation MS-P95 2890 De La Cruz Blvd. Santa Clara, CA 95052 James MacDonald General Research Corporation PO Box 6770 Santa Barbara, CA 93160-6770

M. Goldberg, MS B44-35 Grumman Corporation Bethpage, NY 11714

C. VanOmmersen ICI Explosives USA, Inc. P.O. Box 577 Tamaqua, PA 18252-0577

Guy Spitale
Jet Propulsion Laboratory
California Institute of Technology
Reliability Engineering Section
4800 Oak Grove Drive
Pasadena, CA 91109

Jeff Elder (2)
Kaman Sciences Corporation
Huntsville Office
P. O. Box 2486
Huntsville, AL 35804-2486
Attn: J. Elder, S. Jones

John May Kaman Sciences Corporation 1500 Garden of the Gods Road Colorado Springs, CO 80933

Thomas Grondzik Kendall Square Research 2102 Business Center Drive, Suite 115D Irvine, CA 92715

Kenneth Lockwood Knolls Atomic Power Laboratory General Electric Company PO Box 1072 Schenectady, NY 12301-1072

E. S. Gaffney Ktech Corporation 911E Pennsylvania NE Albuquerque, NM 87112

Ed Cykowski

Lockheed Engineering and Space Company

Mail Code B22 2400 NASA Road 1 Houston, TX 77058-3711

Erik Matheson (2) O/81-12 B/157

Lockheed Missiles & Space Company

1111 Lockheed Way

Sunnyvale, CA 94088-3504

Attn: Y.-I. Choo, E. Matheson

Richard Crawford Logicon RDA

P. O. Box 92500

Los Angeles, CA 90009

John Flowers

LTV Missiles and Electronics Group

P. O. Box 650003

M/S EM-36

Dallas, TX 75265-0003

Tim Gillespie

MS H4330

Martin Marietta Astronautics Group

PO Box 179

Denver, CO 80201

George Christoph

Martin Marietta Laboratories

1450 S. Rolling Road

Baltimore, Maryland 21227

Larry Williams

Martin Marietta

MP 126

Box 5837

Orlando, FL 32855

N. A. Louie

Department Y831, Mail Station 13-3

McDonnell Douglas Missile Space Systems

Company

5301 Bolsa Avenue

Huntington Beach, CA 92647

K. Nelson

Dept. of Chemistry

MIT

77 Massuchessets Ave.

Cambridge, MA 02139

Eric Christiansen

NASA Johnson Space Center

Space Science Branch/SN3

Houston, TX 77058

Scott Hill

NASA Marshall Space Flight Center

Mail Code ED52

Redstone Arsenal

Huntsville, AL 35812

John M. Pipkin (Code 4310)

Naval Coastal Systems Center

Thomas Drive

Panama City Beach, FL 32405-5000

C. T. White

Code 6179

Naval Research Lab

Washington, DC 20375-5000

Naval Surface Warfare Center (10)

10901 New Hampshire Ave.

Silver Spring, MD 20903-5000

Attn: R. D. Bardo

Attn: R. R. Bernecker

Attn: C. S. Coffey

Attn: J. W. Forbes

Attn: H. D. Jones

Attn: H. Mair

Attn: P. Miller

Attn: D. Price

Attn: J. M. Short

Attn: D. G. Tasker

Dan Bowlus

Naval Underwater Systems Center

Mail Code 8123

Newport, RI 02841-5047

Naval Weapons Center (3) China Lake, CA 93555-60001

> Attn: A. L. Atwood, Code 3891 Attn: T. L. Boggs, Code 0239 Attn: E. Lundstrom, Code 3261

D. H. Liebenberg (2) 800 N. Quincy St. Office of Naval Research Arlington, VA 22217 Attn: D. Liebenberg, R. S. Miller

P.-A. Persson CETR New Mexico Tech Socorro, NM 87801

Mark Walz NMI 2229 Main Street Concord, MA 01742

Yasuyuki Horie Box 7908 North Carolina State University Raleigh, NC 27695

Firooz Allahdadi (3)
Phillips Laboratory
PL/WSSD
Kirtland AFB, NM 87117-6008
Attn: F. Allahdadi, D. Fulk, D. Medina

Ray Pierce Physics International PO Box 5010 San Leandro, CA 94577-0599

Keith Pauley PNL KS-42 P. O. Box 999 Richland, WA 99352

1

ŧ

Steve Rieco POD Associates, Inc. 2309 Renard Place, SE Suite 201 Albuquerque, NM 87106 C. W. Nestor, Jr.
Oak Ridge National Laboratory
PO Box 2009
Oak Ridge, TN 37831-8058

D. E. Welch Engineering Techology Division Oak Ridge National Laboratory PO Box 2003 Oak Ridge, TN 37831-7294

Anthony Gurule Orion International Inc. Suite 200 300 San Mateo NE Albuquerque, NM 87108

D. Matuska Orlando Technology, Inc. P. O. Box 855 Shalimar, FL 32579

John Remo Quantametrics, Inc. #1 Brackenwood Path Head of the Harbor St. James, NY 11780

Peter Radkowski, III Radkowski Associates PO Box 5474 Riverside, CA 92517-5474

Tracy Christian-Frear (10) Re/Spec, Inc., Suite 300 4775 Indian School Rd. NE Albuquerque, NM 87110

Greg L. Savoni Rockwell International Corporation 12214 Lakewood Blvd. NA-40 Downey, CA 90241

R&D Associates 6053 West Century Boulevard P.O. Box 92500 Los Angeles, CA 90009 Attn: B. Lee

Mark Fry SAIC/New York 8 West 40th Street 14 Floor New York, New York 10018

Ronald Weitz SAIC 2109 Air Park Road SE Albuquerque, NM 87106

James Zerkle SAIC, M/S C-2 10260 Campus Point Drive San Diego, CA 92121

Charles E. Needham Maxwell/S-CUBED 2501 Yale SE Suite 300 Albuquerque, NM 87106

Steve Peyton S-CUBED P. O. Box 1620 LaJolla, CA 92038-1620

C. E. Anderson (2) Southwest Research Institute P.O. Drawer 28510 San Antonio, TX 78284 Attn.: C. E. Anderson, J. D. Walker

William G. Tanner Space Science Laboratory P. O. Box 97303 Waco, TX 76798

M. Cowperthwaite SRI International 333 Ravenswook Ave. Menlo Park, CA 94025

L. Seaman SRI International 333 Ravenswook Ave. Menlo Park, CA 94025 Bhuminder Singh (2)
Teledyne Brown Engineering
Cummings Research Park
300 Sparkman Dr., NW
PO Box 070007
Huntsville, AL 35807-7007
Attn: B. Singh, B. Loper

Steve Herrick
Textron Defense Systems
Mail Stop 1115
201 Lowell St.
Wilmington, MA 01887

Dwight Clark, Mailstop 280 Thiokol Corporation Advanced Technology Division P. O. Box 707 Brigham City, Utah 84302

Akhilesh Maewal Trans-Science Corporation 7777 Fay Avenue Suite 112 La Jolla, CA 92037

Stan Fink, R1/1044 TRW One Space Park Redondo Beach, CA 90278

T. P. Shivananda TRW Ballistic Missiles Group SB/2/1011 P. O. Box 1310 San Bernardino, CA 92402-1310

Brent Webb Umpqua Research Company P. O. Box 791 125 Volunteer Way Myrtle Creek, OR 97457

Gene Carden University of Alabama PO Box 870278 Tuscaloosa, AL 35487-0278 Gary Hough Aerophysics Research Facility University of Alabama at Huntsville Huntsville, AL 35899

R. Jeanloz
Department of Geology and Geophysics
University of California

Berkeley, CA 94720

David J. Benson Dept. of AMES R-011 University of California San Diego La Jolla, CA 92093

Robert Culp
Department of Aerospace Engineering
Sciences
Campus Box 429
University of Colorado
Boulder, CO 80309

Garry Abfalter Impact Physics Group University of Dayton Research Institute 300 College Park, Room KLA 14 Dayton, OH 45469-0182

G. Ali Mansoori Department of Energy Engineering University of Illinois at Chicago Circle Box 4348 Chicago, IL 60680

Chen-Chi Hsu University of Florida Department of Aerospace Engineering 231 Aerospace Building Gainesville, FL 32611

Murli H. Manghnani Hawaii Institute of Geophysics University of Hawaii Honolulu, Hawaii 96822

Scott Stewart
Department of Theoretical and Applied
Mechanics
University of Illinois
Urbana, Illinois 61801

R.W. Armstrong
Department of Mechanical Engineering
University of Maryland
College Park, MD 20742

R. D. Dick Department of Mechanical Engineering University of Maryland College Park, MD 20742

R. L. McCrory Laboratory for Laser Energetics University of Rochester 250 East River Road Rochester, NY 14623-1299

H. M. Van Horn Department of Physics and Astronomy University of Rochester Rochester, NY 14627

Thomas Moriaty
Department of Engineering Sciences and
Mechanics
University of Tennessee
Knoxville, TN 37996-2030

Stephan J. Bless The University of Texas at Austin Institute for Advanced Technology 4030-2 W. Braker Lane, Suite 200 Austin, TX 78712

Eric Fahrenthold Dept. of Mech. Engineering The University of Texas at Austin Austin, TX 78712

R. A. Schapery
Dept. of Aerospace Engineering
The University of Texas at Austin
Austin, TX 78712

Chadee Persad Institute for Advanced Technology The University of Texas at Austin 4030-2 W. Braker Ln. Austin, TX 78759-5329

Keith Holsapple

Department of Aeronautics and Astronautics

FS10

The University of Washington

Seattle, WA 98195

S. A. Schakelford FJSRL/NC (AFSC)

USAF Academy, CO 80840-6528

Y. M. Gupta

Department of Physics **Shock Dynamics Laboratory** Washington State University Pullman, WA 99164-2814

Wright Laboratory (5)

Eglin AFB, FL 32542-5434

Attn: D. Brubaker Attn: J. A. Collins Attn: J. Foster

Attn: R. L. McKenney Attn: B. Patterson

J. M. McBride

Dept. of Chemistry Yale University P.O. Box 6666 New Haven, CT

J. H. S. Lee

Dept. of Mech. Engineering

McGill University Montreal, Quebec CANADA H3A 2K6

A. Ng

Department of Physics University of British Columbia Vancouver, BC V6T 26A **CANADA**

J. Boileau

Societe Nationale des Poudres et Explosifs

12 Ouai Henri IV 75004 Paris **FRANCE**

R. Cherét

Commissariat à l'Energie Atomique 33

Rue de la Federation

Paris, 75015 **FRANCE**

Centre d'Etudes de Limeil-Valenton (2)

Attn: F. Perrot, M. Penicaud

B.P. 27

F-94190 Villeneuve St. Georges

FRANCE

Centre d'Etudes de Vaujours (4)

Attn: R. Chirat, J. Baute, J. M. Chevalier, L Brun

F-77181 Courtry

FRANCE

D. Bergues

Commissariat à l'Energie Atomique

Centre de'Etudes de Gramat

Gramat, 46500 **FRANCE**

H. N. Presles

ENSMA

Laboratoire d'Energétique et de Détonique

Poitiers (Cedex) 86034

FRANCE

J.-P. Hansen

Ecole Normale Superieure de Lyon

46, allee d'Italie 69364 Lyon Cedex 07

FRANCE

H. Moulard/M. Samirant

Institut Saint Louis 5, rue de l'Industrie BP 34 68301 Saint Louis

FRANCE

M. Held

MBB Schrobenhausen D-8898 Schrobenhausen

GERMANY

F. Hensel

1

1

Fachbereich Physikalische Chemie Philipps-Universitat Marburg Hans-Meerwein-Strasse D-3550 Marburg GERMANY

V. Hohler

Ernst-Mach-Institut Eckerstrasse 4 7800 Freiburg i.BR GERMANY

F. Volk

Fraunhofer-Institut für Chemische Technology D-7507 Pfinztal-Berghausen GERMANY

S. K. Sikka

High Pressure Physics Division Bhabha Atomic Research Centre Trombay, Bombay - 400 085 INDIA

Y. Rosenfeld

Nuclear Research Center - Negev P.O. Box 9001 Beer Sheva ISRAEL

K. Tanaka

National Chemical Lab for Industry Explosives Chemistry Section Tsukuba Ibaraki 305 JAPAN

T. Hikita

Fukui Institute of Technolgy Gakuen, Fukui 910 JAPAN

Y. Kato

Chemicals and Explosives Laboratory Nippon Oil and Fats Co., Ltd. Taketoyo, Aichi 470-23 JAPAN G. A. Leiper
ICI Explosives
Stevenston, Ayshire
SCOTLAND

Fernando Alcalde

Union Espanola De Explosivos

Claudio Coello, 124 Madrid, 28006 SPAIN

J. Campos/J. C. Gois S.A. Eng. Mecanica

Fac. of Science and Technology

University of Coimbra

3000 Coimbru PORTUGAL

A. N. Dremin

Institute of Chemical Physics Chernogolovka, P.O. 142432 Moscow region, RUSSIA

V. I. Fortov

Institute of Chemical Physics Chernogolovka, P.O. 142432 Moscow region, RUSSIA

I. V. Lomonosov

Institute of Chemical Physics Chernogolovka, P.O. 142432 Moscow region, RUSSIA

H. Ostmark FOA Section 243 172 90 Sundbyberg SWEDEN

M. Cook/P. Haskins Defence Research Agency Sevenoaks, Kent UNITED KINGDOM

J. E. Field/M. M. Chaudhri

Dept. of Physics

University of Cambridge

Cavendish Laboratory, Madingley Road

Cambridge CB3 OHE UNITED KINGDOM

B. D. Lambourn Atomic Weapons Establishment Aldermaston, Reading, RG7 4PR Berkshire UNITED KINGDOM

W. Byers Brown University of Manchester Department of Chemistry Manchester, M13 9PL UNITED KINGDOM

Los Alamos National Laboratory (72) Mail Station 5000 P.O. Box 1663 Los Alamos, NM 87545

> Attn: J. Abdallah, MS-212 Attn: T. F. Adams, MS F663 Attn: B. I. Bennett, MS B221 Attn: S. T. Bennion, MS F663 Attn: J. B. Bdzil, MS P952 Attn: W. Birchler, MS G787 Attn: P. J. Blewett, MS F663 Attn: R. J. Bos, P-5 Attn: M. W. Burkett, MS G787 Attn: E. J. Chapyak, MS F663 Attn: R. A. Clark, MS B257 Attn: G. E. Cort, MS G787 Attn: C. W. Cranfill, MS-B257 Attn: B. J. Daly, MS B216 Attn: W. C. Davis, MS-P952 Attn: T. N. Dey, MS-F665 Attn: J. J. Dick, MS-P952 Attn: J. K. Dienes, MS B216 Attn: H. Flaush, MS C936 Attn: C. A. Forest, MS-P952 Attn: R. P. Godwin, MS F663 Attn: F. Harlow, MS B216 Attn: W. B. Harvey, MS F663 Attn: B. L. Holian, MS J569 Attn: K. S. Holian, MS B295 Attn: J. W. Hopson, MS B216 Attn: H. Horak, MS C936

Attn: M. L. Hudson, MS J970 Attn: E. S. Idar, MS-J960 Attn: J. D. Johnson, MS-B221 Attn: J. N. Johnson, MS-B221 Attn: N. L. Johnson, MS B216 Attn: J. E. Kennedy, MS-B950 Attn: J. F. Kerrisk, MS G787 Attn: M. Klein, MS F669 Attn: D. Kothe, MS-B216 Attn: R. A. Krajcik, MS-F218 Attn: W. H. Lee, MS B226 Attn: R. A. Lesar, MS-B262 Attn: L. B. Luck, MS-K557 Attn: C. L. Mader, MS-B214 Attn: J. M. Mack, MS-P940 Attn: D. Mandell, MS F663 Attn: L. G. Margolin, MS D406 Attn: G. H. McCall, MS B218 Attn: J. K. Meier, MS G787 Attn: R. W. Meier, MS G787 Attn: A. L. Merts, MS-212 Attn: C. E. Morris, MS-J970 Attn: T. R. Neal, MS-P940 Attn: A. T. Oyer, MS G787 Attn: D. A. Poling, MS-F669 Attn: C. E. Ragan, MS-D449 Attn: J. Ramsay, MS-J960 Attn: M. Rich, MS F669 Attn: J. P. Ritchie, MS-B214 Attn: M. Sahota, MS B257 Attn: G. L. Schott, MS P952 Attn: B. P. Shafer, MS-K574 Attn: J. W. Shaner, MS-J970 Attn: D. H. Sharp, MS-B285 Attn: S. Shaw, MS-B214 Attn: S. A. Sheffield, MS-P952 Attn: W. Sparks, MS F663 Attn: C.B. Storm, P915 Attn: G. K. Straub, MS-B221 Attn: P. K. Tang, MS-F664 Attn: M. T. Thieme, MS-F664 Attn: D. Tonks, MS B221 Attn: H. E. Trease, MS B257 Attn: J. D. Wackerle, MS-P952 Attn: L. Witt, MS C936

University of California (31)
Lawrence Livermore National Laboratory
7000 East Ave.
P.O. Box 808
Livermore, CA 94550

Attn: A. Attia, L-200 Attn: D. E. Burton, L-18 Attn: R. B. Christensen, L-35 Attn: G. R. Gathers, L368 Attn: H. C. Graboske, L-296 Attn: L. G. Green, L-282 Attn: R. Grover, L-299 Attn: J. W. Kury, L-368 Attn: J. M. LeBlanc, L-35 Attn: E. L. Lee, L-368 Attn: D. A. Liberman, L-477 Attn: A. K. McMahan, L-299 Attn: W. Moran, L-200 Attn: R. M. More, L-321 Attn: M. J. Murphy, L-368 Attn: W. J. Nellis, L-299 Attn: A. L. Nichols, L-368 Attn: W. Quirk, L-35 Attn: J. E. Reaugh, L-290 Attn: F. H. Ree, L-299 Attn: C. E. Rosenkilde, L-84 Attn: M. Ross, L-299 Attn: R. L. Simpson, L-282 Attn: P. C. Souers, L-368 Attn: D. J. Steinberg, L-35 Attn: W. C. Tao, L-282 Attn: C. M. Tarver, L-368 Attn: R. E. Tipton, L-35 Attn: M. van Thiel, L-299 Attn: M. Wilkins, L-321 Attn: D. A. Young, L-299

ì

Internal Distribution

G. A. Samara 1153 R. A. Graham 1153 1153 A. C. Switendick M. A. Sweeney 1241 M. K. Matzen 1271 G. O. Allshouse 1271 E. J. McGuire 1271 1400 E. H. Barsis S. S. Dosanih 1402 J. A. Ang 1404 J. N. Jortner 1408 G. S. Davidson 1415 W. J. Camp 1421 1422 R. Allen 1423 E. F. Brickell A. L. Hale 1424 J. H. Biffle 1425 J. M. McGlaun 1431 1431 K. G. Budge M. G. Elrick 1431 E. S. Hertel 1431 J. S. Pecry 1431

1431 S. V. Petney
 1431 A. C. Robinson
 1431 T. G. Trucano
 1431 M. Wong

1431 CTH Day File1432 P. Yarrington1432 R. L. Bell

1432 R. M. Brannon1432 P. J. Chen

1432 H. E. Fang1432 A. V. Farnsworth1432 G. I. Kerley (10)

1432 M. E. Kipp1432 F. R. Norwood

1432 S. A. Silling1432 P. A. Taylor1433 P. L. Stanton

1433 P. L. Stanton 1433 M. Boslough 1433 D. A. Crawford

1433 L. C. Chhabildas1433 M. D. Furnish

1433 D. E. Grady1434 D. Martinez

1511 J. S. Rottler

1512 A. C. Ratzel

- 1512 M. R. Baer
- 1512 M. L. Hobbs
- 1513 R. D. Skocypec
- 1553 W. L. Hermina
- 1561 H. S. Morgan
- 1562 R. K. Thomas
- 2512 J. G. Harlan
- 2513 D. E. Mitchell
- 2513 S. G. Barnhart
- 2513 S. H. Fischer
- 2513 S. M. Harris
- 2513 M. G. Vigil
- 2514 L. L. Bonzon
- 2514 A. M. Renlund
- 2514 L. J. Weirick
- 5166 R. E. Setchell
- 5602 J. R. Asay
- 6111 J. L. Wise
- 6117 W. R. Wawersik
- 6119 R. W. Ostensen
- 6418 S. L. Thompson
- 6418 N. Kmetyk
- 6515 N. Berman
- 6515 K. Noyack
- 8741 G. A. Benedetti
- 8741 M. L. Chiesa
- 8741 L. E. elker
- 8742 J. J. Di. :
- 8243 M. L. Callabresi
- 8743 D. J. Bammann
- 8745 R. J. Kee
- 9311 A. J. Chabai
- 9311 T. Bergstresser
- 9333 P. W. Cooper
- 9702 T. Hitchcock
- 9722 R. O. Nellums
- 9723 J. M. Holovka
- 9723 M. J. Forrestal
- 8523-2 Central Technical Files
- 7151 Technical Publications
- 7131 Toomboa Tabilotto
- 7613-2 Document Processing for DOE/OSTI

Technical Libarary (5)

(10)

7141

ί.

